論文 / 著書情報
Article / Book Information

題目(和文)	単結晶, 粗大結晶粒および超微細結晶粒を持つアルミニウムの低温域における繰り返し変形と内部組織
Title(English)	Low-temperature cyclic deformation and microstructure of single-crystalline,coarse-grained and ultrafine-grained aluminum
著者(和文)	中西如人
Author(English)	Yukito Nakanishi
出典(和文)	学位:博士(工学), 学位授与機関:東京工業大学, 報告番号:甲第9143号, 授与年月日:2013年3月26日, 学位の種別:課程博士, 審査員:加藤 雅治
Citation(English)	Degree:Doctor (Engineering), Conferring organization: Tokyo Institute of Technology, Report number:甲第9143号, Conferred date:2013/3/26, Degree Type:Course doctor, Examiner:
学位種別(和文)	博士論文
Type(English)	Doctoral Thesis

Low-Temperature Cyclic Deformation and Microstructure of Single-Crystalline, Coarse-Grained and Ultrafine-Grained Aluminum

A Dissertation for the Degree
Doctor of Engineering
Materials Science and Engineering

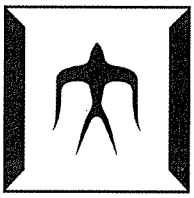

Department of Materials Science and Engineering
Interdisciplinary Graduate School of Science and Engineering
Tokyo Institute of Technology

Yukito NAKANISHI

February, 2013

Contents

Chapter 1. *General introduction*

1.1 Preface 1

1.1.1 Fatigue of materials 1

1.1.2 Ultrafine-grained metals 2

1.2 The overall objective of present dissertation 3

1.3 The outline of this dissertation 3

References 5

Chapter 2. *Cyclic deformation behavior and microstructure of fcc metals: survey and perspective*

2.1 Cyclic hardening in fcc metals 7

2.2 Cyclic deformation behavior and microstructure of single-crystalline fcc metals 8

2.3 Cyclic deformation behavior and microstructure of coarse-grained fcc metals 10

2.4 Cyclic deformation behavior and microstructure of ultrafine-grained fcc metals 11

2.5 Research needed 12

References 13

Chapter 3. *Low-temperature cyclic deformation and microstructure of single-crystalline aluminum*

3.1 Introduction 22

3.2 Experimental procedure 23

3.3 Results 24

3.3.1 Cyclic deformation behavior of Al single crystals 24

3.3.2 Surface observation 25

3.3.3 Microstructural observation 25

3.4 Discussion

3.4.1 Dependence of the channel width on shear stress amplitude 26

3.4.2 Effects of test temperature, stress direction and SFE on cyclic deformation behavior 28

3.5 Conclusions 29

References 31

Chapter 4. *Low-temperature cyclic deformation and microstructure of ultrafine-grained aluminum*

4.1 Introduction 41

4.2 Experimental procedure 42

4.2.1 Equal channel angular pressing 42

4.2.2 Specimen preparation 42

4.2.3 Fatigue tests 43

4.2.4 Microstructural observation 44

4.3 Results and discussion 44

4.3.1 Cyclic hardening and softening 44

4.3.2 Shear band formation 44

4.3.3 Microstructural observation 45

4.3.4 Dependence of the channel width on stress amplitude 46

4.4 Conclusions 47

References 48

Chapter 5. *Stability of fatigued dislocation wall structure in coarse-grained and ultrafine-grained aluminum against monotonic tensile deformation*

5.1 Introduction 59

5.2 Experimental procedure 60

5.3 Results 62
5.3.1 Cyclic deformation behavior of CG and UFG Al 62
5.3.2 Monotonic tensile deformation behavior of fatigued Al 62
5.3.3 Microstructural observation 63
5.4 Discussion 64
5.4.1 Dependence of the channel width on stress amplitude 64
5.4.2 Relationship between monotonic tensile deformation behavior and microstructural stability of CG and UFG Al 65
5.5 Conclusions 67
References 69

Chapter 6. *General conclusions*

6.1 Summary and conclusions of the present dissertation 80
6.2 Future studies 82

Acknowledgements 84

Chapter 1
General introduction

1.1 Preface

1.1.1 Fatigue of materials

Researches on fatigue have been conducted since nineteenth century. Fatigue of materials is a fracture phenomenon that occurs when materials subjected cyclic loads where a single load would not do any harm. Historically, the first occurrence of fatigue is connected with industrial products subjected to cyclic deformation: sailing vessel, railway and steam turbines. Mughrabi mentioned in his paper [1] that the purpose of early studies was to determine the number of cyclic loadings applicable until failure occurred in stress-amplitude controlled tests [2-4] and, that little attention was paid to the microscopic origin of fatigue damage. In 1903, Ewing and Humfrey [5] demonstrated that slip bands appeared on the surface of specimens during cyclic deformation and those bands gradually developed into crack. Later, Coffin [6] and Manson [7] showed that the fatigue process is conditioned by cyclic plastic deformation.

According to Fine [8], the progression of fatigue damage in materials is divided into the following stages:

(1) Property and microstructural changes caused by cyclic plastic deformation
(2) Initiation of microcracks
(3) Growth of microcracks to form a macrocrack
(4) Propagation of macrocracks

The conditions for the initiation of microcracks and rate of crack propagation are strongly

influenced by a wide range of mechanical, microstructural and environmental factors [9]. Additionally, it is well known that a fatigue crack can be formed at early phase and large part of fatigue life is occupied by crack growth [10-13]. Therefore, it is important to understand what occurs in the material before the fatigue crack initiation and how microstructural or environmental factors affect cyclic deformation behavior. With the advances in electron microscopy, substantial progress has been made in revealing cyclic deformation behavior and microstructural development [9, 14-16]. As will be discussed in Chapter 2, numerous studies on cyclic deformation of single-crystalline and polycrystalline metals have been performed.

1.1.2 Ultrafine-grained metals

Strength of materials is a fundamental factor in mechanical properties of structural materials. For many decades, grain refinement has been practiced as an effective means to enhance the strength of materials [17, 18]. Until several decades ago, there was a limit to reducing the grain size in bulk materials below about 10 μm [19]. With the development of a number of so-called severe plastic deformation (SPD) techniques, it has become available for producing bulk materials with grain sizes D in the range of roughly 100 nm < D < 1 μm, referred to as ultrafine-grained (UFG) materials. SPD techniques break down the microstructure into finer and finer grains by introducing a large amount of strain. Now many SPD techniques have been developed: equal channel angular pressing (ECAP) [20, 21], accumulate roll-bonding (ARB) [22, 23], high-pressure torsion (HPT) [24, 25] and multi-directional forging (MDF) [26, 27].

The strength of UFG metals is several times as high as that of coarse-grained (CG) fcc metals (D > 10 μm) [19, 27-33]. In addition, UFG materials show extraordinary properties that have never seen in CG materials: for example, yield-drop-phenomenon in pure metals [33, 34], easy occurrence of recovery and recrystallization [35-37], high strain-rate sensitivity [38, 39] and inverse temperature dependence of activation volume [40]. Cyclic deformation behavior of UFG metals is also different from that of single-crystalline and CG

metals, as will be shown in Chapter 2.

1.2 The overall objective of present dissertation

The overall objective of the present dissertation is to obtain comprehensive understanding about cyclic deformation behavior of single-crystalline, CG and UFG Al, and to investigate the effects of test temperature on cyclic deformation behavior. The main focuses are placed on the investigation of the following subjects.

(1) To clarify key factors which affect the characteristic cyclic deformation behavior and microstructural development in pure Al
(2) To make a detailed investigation on cyclic deformation behavior of UFG Al
(3) To investigate the stability of fatigued dislocation structure in CG and UFG Al against monotonic tensile deformation

1.3 The outline of this dissertation

The present dissertation consists of the following six chapters.

In Chapter 1, "General Introduction", the backgrounds of the present dissertation are described. The overall objectives and outline in this dissertation are also shown.

In Chapter 2, "Cyclic deformation behavior and microstructure of fcc metals: survey and perspective", attention is focused on the fundamental cyclic deformation behavior and microstructural development of single crystalline, CG and UFG fcc metals. In addition, the purpose and importance of the present study is also described.

In Chapter 3, "Low-temperature cyclic deformation of aluminum single crystals", the cyclic deformation behavior and microstructural development of Al single crystals fatigued at 77 K are investigated. The dependence of the saturation stress amplitude on saturation

channel width between adjacent dislocation walls is analyzed. The effects of homologous temperature and stacking fault energy on cyclic deformation behavior and microstructural development are also discussed.

In Chapter 4, "Low-temperature cyclic deformation of UFG aluminum", low-cycle strain-controlled fatigued tests have been carried out for UFG Al at various temperatures between 300 K and 83 K. Temperature dependence of cyclic deformation behavior and microstructural development in UFG Al are discussed.

In Chapter 5, "Stability of fatigued dislocation wall structure in CG and UFG aluminum against monotonic tensile deformation", monotonic tensile tests are carried for CG and UFG Al at 300 K and 77 K soon after strain-controlled fatigue tests at 77 K. The effects of fatigue tests on succeeding monotonic tensile deformation behavior of CG and UFG Al are investigated. Stability of fatigued dislocation wall structures in CG and UFG Al against monotonic tensile deformation is discussed.

In Chapter 6, "General conclusions", main results and conclusions obtained in the present dissertation are summarized and remarkable future studies are introduced.

References

[1] H. Mughrabi: Metall. Mater. Trans. A **42** (2009) 1257-1279.

[2] W. Fairbairn: Philos. Trans. R. Soc. **54** (1864) 311-325.

[3] A. Wöhler: Z. Bauwesen **20** (1870) 73-106.

[4] O. H. Basquin: Proc. ASTM **10** (1910) 625-630.

[5] J. A. Ewing and J. C. W. Humfrey: Philos. Trans. R. Soc. **200** (1903) 241-250.

[6] L. F. Coffin: Trans. ASME **76** (1954) 931-950.

[7] S. S. Manson: National Advisory Committee on Aerospace Technical Note 2933, National Advisory Committee, (Cleveland, 1954).

[8] M. E. Fine: Metall. Trans. A **11** (1980) 365-379.

[9] S. Suresh: *Fatigue of materials*, 1st ed., (Cambridge, 1998).

[10] H. D. Solomon: J. Mater. **7** (1972) 299-306.

[11] D. F. Mowbray: ASTM STP **601** (1976) 33-46.

[12] Y. Murakami, S. Harada, T. Endo, H. Tanishi and Y. Fukushima: Eng. Fract. Mech. **18** (1983) 909-924.

[13] T. Hoshide, T. Yamada and S. Fujimura: Eng. Fract. Mech. **21** (1985) 85-101.

[14] Z. F. Zhang and Z. G. Wang: Prog. Mater. Sci. **53** (2008) 1025-1099.

[15] P. Li, S. X. Li, Z. G. Wang and Z. F. Zhang: Prog. Mater. Sci. **56** (2011) 328-377.

[16] M. Sauzay and L. P. Kubin: Prog. Mater. Sci. **56** (2011) 725-784.

[17] E. O. Hall: Proc. Phys. Soc. London B **64** (1951) 747-753.

[18] N. J. Petch: J. Iron Steel Inst. London **174** (1953) 25-28.

[19] H. Mughrabi and H. W. Höppel: Int. J. Fatigue **32** (2010) 1413-1427.

[20] Y. Iwahashi, Z. Horita, M. Nemoto and T. G. Langdon: Acta Mater. **46** (1998) 3317-3331.

[21] T. G. Langdon: J. Mater. Sci. **42** (2007) 3388-3397.

[22] Y. Saito, N. Tsuji, H. Utsunomiya and S. Tanigawa: Scr. Mater. **39** (1998) 1221-1227.

[23] N. Tsuji, Y. Saito, S. H. Lee and Y. Minamino: Adv. Eng. Mater. **5** (2003) 338-344.

[24] A. P. Zhilyaev, B.-K. Kim, J. A. Szpunar, M. D. Baró and T. G. Langdon: Mater. Sci. Eng. A **391** (2005) 377-389.

[25] Z. Horita and T. G. Langdon: Mater. Sci. Eng. A **410-411** (2005) 422-425.

[26] T. Sakai, H. Miura and X. Yang: Mater. Sci. Eng. A **499** (2009) 2-6.

[27] K. B. Nie, K. Wu, X. J. Wang, K. K. Deng, Y. W. Wu and M. Y. Zheng: Mater. Sci. Eng. A **527** (2010) 7364-7338.

[28] C. Y. Yu, P. W. Kao and C. P. Chang: Acta Mater. **53** (2005) 4019-4028.

[29] J. May, D. Amberger, M. Dinkel, H. W. Höppel and M. Göken: Mater. Sci. Eng. A **483-484** (2008) 481-484.

[30] N. Kamikawa, X. Huang, N. Tsuji and N. Hansen: Acta Mater. **57** (2009) 4198-4208.

[31] M. Kato: Mater. Sci. Eng. A **516** (2009) 64-69.

[32] A. Yoshida, Y. Miyajima and S. Onaka: Mater. Trans. **53** (2012) 23-26.

[33] C. Y. Yu, P. W. Kao and C. P. Chang: Acta Mater. **53** (2005) 4019-4028.

[34] N. Kamikawa, X. Huang, N. Tsuji and N. Hansen: Acta Mater. **57** (2009) 4198-4208.

[35] X. Molodova, G. Gottstein, M. Winning and R. J. Hellmig: Mater. Sci. Eng. A **460-461** (2007) 204-213.

[36] Y. Zhang, J. T. Wang, C. Cheng and J. Liu: J. Mater. Sci. **43** (2008) 7326-7330.

[37] H. W. Zhang, X. Huang, R. Pippan and N. Hansen: Acta Mater. **58** (2010) 1698-1707.

[38] Q. Wei, S. Cheng, K. T. Ramesh and E. Ma: Mater. Sci. Eng. A **381** (2004) 71-79.

[39] T. Kunimine, N. Takata, N. Tsuji, T. Fujii, M. Kato and S. Onaka: Mater. Trans. **50** (2009) 64-69.

[40] T. Kunimine, T. Aragaki, T. Fujii, S. Onaka and M. Kato: J. Mater. Sci. **46** (2011) 4302-4307.

Chapter 2

Cyclic deformation behavior and microstructure of fcc metals: survey and perspective

2.1 Cyclic hardening in fcc metals

When well-annealed fcc single crystals oriented for single slip are subjected to cyclic deformation under fully reversed low-cycle strain-controlled tests, rapid cyclic hardening (that is, a rapid increase in flow stress with increasing number of fatigue cycle) is known to occur. The hardening rate decreases with increasing number of cycles. For fcc single crystals, except for Al, the flow stress reaches a quasi-steady state, known as saturation. Once the saturation occurs, the shear stress amplitude τ_a remains unchanged by further cycling.

It is well known that the plastic strain causes irreversible changes in the material substructure, mainly in the dislocation structure, and is the most decisive phenomenon in the fatigue process. Therefore, it is reasonable that fatigue damage is evaluated by the accumulation of plastic strain. A nominal measure of damage accumulation under fully-reversed plastic-strain-controlled fatigue tests is cumulative plastic shear strain γ_{cum}, defined as

$$\gamma_{cum} = 4N\gamma_{pl} \tag{2-1}$$

where N is the number of fatigue cycles and γ_{pl} is plastic shear strain amplitude.

On the other hand, polycrystalline metals consist of many grains with different relative crystallographic orientation. The stress at which slip begins in each grain depends on its orientation with respect to the loading axis, following the Schmid law. The slip systems with higher Schmid factors are activated even if the strain amplitudes are not high.

For comparison of the fatigue behavior of single crystals with that of polycrystals, plastic tensile strain amplitude ε_{pl}, tensile stress amplitude σ_a and cumulative plastic tensile strain ε_{cum} of a polycrystalline metals are evaluated as follows

$$\varepsilon_{pl} = \frac{\gamma_{pl}}{M} \tag{2-2}$$

$$\sigma_a = M\tau_a \tag{2-3}$$

$$\varepsilon_{cum} = 4N\varepsilon_{pl} \tag{2-4}$$

where M is a Taylor factor of 3.06 for fcc metals.

In the following, plastic-strain controlled cyclic deformation behavior of fcc metals, mainly pure Cu and pure Al, will be reviewed briefly for the purpose of making the background of the present dissertation studies clear. Both of the terms "cyclic deformation" and "fatigue" will be used equally since the so-called "low-cycle fatigue" is often performed by the strain-controlled cyclic deformation tests [1-5].

2.2 Cyclic deformation behavior and microstructure of single-crystalline fcc metals

In fcc metals, Cu is the most widely and systematically investigated. Cu single crystals oriented for single slip show hardening followed by saturation under constant plastic-strain-controlled fatigue tests at room temperature (Fig. 2-1) [6-11]. A plot of the saturation shear stress as a function of plastic shear strain amplitude provides the cyclic stress-strain curve (CSSC). The CSSC can be clearly divided into three regions, marked A, B and C in Fig. 2-2: region A ($\gamma_{pl} < 6.5\times10^{-5}$); the saturation stress increases with increasing plastic strain amplitude, region B ($6.5\times10^{-5} \leq \gamma_{pl} \leq 7.5\times10^{-3}$); the saturation stress of 28 MPa is independent of the plastic strain amplitude (so-called "plateau") and region C ($\gamma_{pl} > 7.5\times10^{-3}$); the saturation stress increases again with increasing the plastic strain amplitude. It is known that characteristic dislocation structure is formed in each region. In region A, the matrix vein

structure is formed [6-9, 12]. Figure 2-3 shows an example of the vein structure in a Cu single crystal oriented for single slip [13]. The vein structure is composed of edge dislocations of opposite sign (dislocation dipoles) on primary slip system. In region B, deformation becomes inhomogeneous and persistent slip bands (PSBs) are formed. In this region, the matrix vein and the PSB ladder structures coexist [7-12]. Figure 2-4 shows an example of the matrix vein and PSB ladder structures [13]. The PSB ladder walls are made up dominantly of edge dislocations on the primary slip system and are perpendicular to the primary slip direction. The plastic deformation in the channels between the ladder walls occurs the backward and forward motion of screw dislocation [14]. The PSBs are much softer than the matrix [15]. Therefore, the PSBs convey much higher plastic strain than the matrix and the plastic strain amplitudes and the volume fraction of PSBs increases linearly with increasing plastic strain amplitude from 0 % (at $\gamma_{pl} = 6.5\times10^{-5}$) to 100 % (at $\gamma_{pl} = 7.5\times10^{-3}$) [16]. In region C, the contribution of secondary slip systems becomes pronounced and labyrinth and cell structures are formed [8, 11, 12]. Figures 2-5 (a) and (b) are transmission electron microscope (TEM) images of labyrinth and cell structures in Cu single crystals oriented for single slip [13]. Dislocation walls of labyrinth structure are parallel to the (001) and (010) planes. The two {100} dislocation walls of the labyrinth structure are formed by the activation of the primary and critical slip systems [17]. The cell structure is formed by the activation of multi slip systems. The plastic deformation occurs by the bowing screw dislocations at the cell walls towards adjacent cell walls and screw dislocations are annihilated by dynamic recovery [18, 19].

Cyclic deformation behavior of Al single crystals is quite different from that of Cu single crystals oriented for single slip. Al single crystals oriented for single, double and multi slips show hardening followed by softening and secondary hardening at room temperature (Fig. 2-1) [20-25]. The cyclic softening is due to the ease of the cross slip activity of Al. Al single crystals oriented for double slip where the Schmid factor of cross slip system is zero show no significant cyclic softening [24]. For Al single crystals, dislocation structure cannot be characterized by the shear plastic strain amplitude. Though

vein and labyrinth structures are formed, cell structure is dominantly formed at any plastic strain amplitude or crystal orientation [22-26]. Neither stress saturation nor ladder structure has been observed at room temperature.

The differences in cyclic deformation behavior and development of microstructure at room temperature between Cu and Al have been explained by considering the difference in stacking fault energy (SFE), reported values being 41 mJ/m^2 for pure Cu [27] and 122 mJ/m^2 for pure Al [28], and homologous temperature, T/T_m where T and T_m are the test temperature and melting point, respectively. Ni and Ag single crystals with SFE of 95 mJ/m^2 [29] and 16 mJ/m^2 [27] show similar cyclic deformation behavior to that of Cu: stress saturation, stress plateau and ladder structure [30-36]. At 77 K, Al single crystals show stress saturation in cyclic hardening curves and stress plateau in CSSCs [20, 37].

2.3 Cyclic deformation behavior and microstructure of coarse-grained fcc metals

Since grains in polycrystalline metals have various different crystal orientations, activation of secondary and multiple slip systems becomes easier in polycrystalline metals than in single crystalline metals oriented for single slip. For coarse-grained (CG) Cu, saturation stress amplitude monotonically increases with increasing the controlled strain amplitude and either weak or no stress plateau has been observed in CSSC [37-40]. Numerous studies demonstrated that typical dislocation structures have been observed such as vein, wall, PSB ladder, labyrinth and cell structures [38, 40-42]. However, the labyrinth and cell structures have been observed at lower strain amplitudes in CG Cu than in single-crystalline Cu oriented for single slip [38, 41, 42].

The cyclic deformation behavior and microstructural development of CG Al is similar to that of single-crystalline Al. CG Al shows hardening followed by softening and secondary hardening [43-45]. However, the amount of cyclic softening in CG Al is insignificant [43-45]. As is the case of single-crystalline Al, cell structure is dominantly formed in CG Al [19, 46]

2.4 Cyclic deformation behavior and microstructure of ultrafine-grained fcc metals

It is known that ultrafine-grained (UFG) metals show characteristic cyclic deformation behavior. The main results obtained in the early studies of cyclic deformation of UFG metals can be summarized as follows:

(1) High cyclic stress: For CG metals, there is no significant dependence of grain size on the cyclic stress [46-48]. However, in the regime of very small grain size below a few micrometers, cyclic stress becomes strongly dependent on grain size [49-51]. The cyclic stress on low-cycle strain-controlled fatigue tests in UFG metals is about 2-4 times larger than that in CG metals [19, 51-53].

(2) Fatigue life: The fatigue lives of UFG metals were generally found to be larger than those of CG metals in high-cycle stress-controlled fatigue tests [46, 51-58]. On the other hand, UFG metals show shorter fatigue lives than CG metals in strain-controlled low-cycle fatigue tests [46, 51, 56-58]. When considering fatigue lives, it is generally understood that fatigue lives in high-cycle fatigue tests are controlled by strength, whereas ductility is a dominant factor in low-cycle fatigue tests [59, 60].

(3) Cyclic softening: UFG Cu and Al show slight hardening followed by cyclic softening and no stress saturation is observed in strain-controlled fatigue tests [46, 51-56, 61-64].

(4) Shear bands formation: During both stress-controlled and strain-controlled fatigue tests, macroscopic shear bands, extending over much larger distances than the UFG grain size, are formed on the surface and fatigue cracks initiate in these shear bands [46, 51-57, 64-67].

(5) Local grain coarsening: Local grain growth occurs even at room temperature, in particular during strain-controlled fatigue tests. Dislocation structures, such as wall and cell structures, are formed only in coarsened grains at room temperature [51-54, 62, 64].

2.5 Research needed

As shown in Section 2.2, the cyclic deformation behavior of Al single crystals is quite different from that of Cu single crystals. In order to obtain comprehensive understanding of fatigue mechanisms for fcc metals, it is essential to elucidate the origin of the differences in the cyclic deformation behavior of Cu and Al. The differences in cyclic deformation behavior and microstructure at room temperature between Cu and Al have been explained by considering as follows

(1) The difference in SFE

(2) The difference in homologous temperature

In this dissertation, the effect of homologous temperature on cyclic deformation behavior and microstructural development of Al will be examined.

As mentioned earlier, UFG metals show characteristic cyclic deformation behavior such as cyclic softening, shear band formation and local grain coarsening. However, the origin of such characteristic cyclic deformation behavior has not been understood. Therefore, further studies on fatigue of UFG metals are needed for understanding the fatigue mechanisms.

References

[1] L. F. Coffin: Trans. ASME **76** (1954) 931-950.

[2] S. S. Manson: National Advisory Committee on Aerospace Technical Note 2933, National Advisory Committee, (Cleveland 1954).

[3] K Bhanu Sankara Rao, M Valsan, R Sandhya, S. K Ray, S L Mannan and P Rodnguez: Int. J. Fatigue **7** (1985) 141-147.

[4] W. Schütz: Eng. Fract. Mech. **54** (1996) 263-300.

[5] X. Z. Lin and D. L. Chen: Mater. Sci. Eng. A **496** (2008) 106-113.

[6] H. Mughrabi: Mater. Sci. Eng. **33** (1978) 207-223.

[7] Z. S. Basinski, A. S. Korbel and S. J. Basinski: Acta Metall. **28** (1980) 191-207.

[8] N. Y. Jin: Acta. Metall. **37** (1989) 2055-2066.

[9] U. Holzwarth and U. Essmann: Appl. Phys. A **58** (1994) 197-210.

[10] J. Bretschneider, C. Holste and W. Kleinert: Mater. Sci. Eng. A **191** (1995) 61-72.

[11] C. Watanabe, K. Kanmuri, M. Kato, S. Onaka and T. Fujii: Philos. Mag. A **82** (2002) 855-866.

[12] C. Laird: Mater. Sci. Eng. **81** (1986) 433-450.

[13] T. Fujii and M. Kato: Private communications (2012).

[14] L. M. Brown: Mater. Sci. Eng. A **285** (2000) 35-42.

[15] O. Helgeland: J. Inst. Met. **93** (1965) 570-575.

[16] A. T. Winter: Philos. Mag. **30** (1974) 719-738.

[17] N. Y. Jin and A. T. Winter: Acta Metall. **32** (1984) 989-995.

[18] C. E. Feltner and C. Laird: Acta Metall. **15** (1967) 1633-1653.

[19] Y. El-Madhoun, A. Mohamed and M. N. Bassim: Mater. Sci. Eng. A **359** (2003) 220-227.

[20] O. Vorren and N. Ryum: Acta Metall. **35** (1987) 855-866.

[21] O. Vorren and N. Ryum: Acta Metall. **36** (1988) 1443-1453.

[22] M. Videm and N. Ryum: Mater. Sci. Eng. A **219** (1996) 1-10.

[23] J. Wang, Z. G. Zhu, Q. F. Fang and G. D. Liu: Mater. Res. Bull. **34** (1999) 1729-1739.

[24] T. Fujii, N. Sawatari, S. Onaka and M. Kato: Mater. Sci. Eng. A **387-389** (2004) 486-490.

[25] P. Li, S. Li, Z. Wang and Z. Zhang: Metall. Mater. Trans. A **41** (2010) 2532-2537.

[26] T. Zhai, J. W. Martin and G. A. D. Briggs: Acta Mater. **44** (1996) 1729-1739.

[27] D. J. H. Cockayne, M. L. Jenkins and I. L. F. Ray: Philos. Mag. **24** (1974) 1383-1392.

[28] V. Yamakov, D. Wolf, M. Salazar, S. R. Phillpot and H. Gleiter: Acta. Mater. **49** (2001) 2713-2722.

[29] P.C.J. Gallagher: Metall. Trans. **1** (1970) 2429-2461.

[30] J. Bretschneider, C. Holste and W. Kleinert: Mater. Sci. Eng. A**191** (1995) 61-72

[31] A. Schwab, J. Bretschneider, C. Buque, C. Blochwitz and C. Holste: Philos. Mag. Lett. **74** (1996) 449-454.

[32] J. Bretschneider, C. Holste and B. Tippelt: Acta. Mater. **45** (1997) 3775-3783.

[33] P. Li, Z. F. Zhang, S. X. Li and Z. G. Wang: Acta Mater. **56** (2008) 2212-2222.

[34] P. Li, Z. F. Zhang, S. X. Li and Z. G. Wang: Scripta Mater. **59** (2008) 730-733.

[35] P. Li, Z. F. Zhang, S. X. Li and Z. G. Wang: Philos. Mag. **89** (2009) 2903-2920.

[36] P. Li, Z. F. Zhang, S. X. Li, Z. G. Wang and Z. G. Wang: Acta Mater. **57** (2009) 4845-4854.

[37] A. Giese and Y. Estrin: Scr. Mater. **28** (1993) 803-807.

[38] K. V. Rasmussen and O. B. Pedersen: Acta Metall. **28** (1980) 1467-1478.

[39] O. B. Pedersen, K. V. Rasmussen and A. T. Winter: Acta Metall. **30** (1982) 57-62.

[40] V. T. Kuokkala and P. Kettunen: Acta Metall. **33** (1985) 2041-2047.

[41] C. D. Liu, M. N. Bassim and D. X. You: Acta Metall. Mater. **42** (1994) 3695-3704.

[42] A. T. Winter, O. B. Pedersen and K. V. Rasmussen: Acta Metall. **29** (1981) 735-748.

[43] M. H. Raymond and L. F. Coffin: Acta Metall. **11** (1963) 801-807.

[44] A. Giese, A. Styczynski and Y. Estrin: Mater. Sci. Eng. A **124** (1990) L11-L13.

[45] M. Videm and N. Ryum: Mater. Sci. Eng. A **219** (1996) 11-20.

[46] M. K. Wong, W. P. Kao, J. T. Lui, C. P. Chang and P.W. Kao: Acta Mater. **55** (2007) 715-725.

[47] H. Haddou, M. Risbet, G. Marichal and X. Feaugas: Mater. Sci. Eng. A **379** (2004) 102-111.

[48] J. Zhang and Y. Jiang: Int. J. Plasticity **22** (2006) 536-556.

[49] E. Theile, C. Holste and R. Klemm: Z. Metallkd **93** (2002) 730-736.

[50] C. Holste: Philos. Mag. **84** (2004) 299-315.

[51] H. Mughrabi and H. W. Höppel: Int. J. Fatigue **32** (2010) 1413-1427.

[52] S. R. Agnew and J. R. Weertman: Mater. Sci. Eng. A **244** (1998) 145-153.

[53] H. Mughrabi and H. W. Höppel: Mat. Res. Sym. Proc. **634** (Erlangen, 2001) B2.2.1-B2.2.11.

[54] H. W. Höppel, M. Brunnbauer, H. Mughrabi, R. Z. Valiev and A. P. Zhilyaev: Proc. Materials Week 2000, (Wiley-VCH, 2001) http://www.materialsweek.org/ proceedings.

[55] L. Kunz, P. Lukáš and M. Svoboda: Mater. Sci. Eng. A **424** (2006) 97-104.

[56] J. May, D. Amberger, M. Dinkel, H. W. Höppel and M. Göken: Mater. Sci. Eng. A **483-484** (2008) 481-484.

[57] P. Lukáš, L. Kunz, L. Navrátilová and O. Bokůvka: Mater. Sci. Eng. A **528** (2011) 7036-7040.

[58] S. Malekjani, P. D. Hodgson, P. Cizek, I. Sabirov and T. B. Hilditch: Int. J. Fatigue **33** (2011) 700-709.

[59] H. W. Höppel, C. Xu, M. Kautz, N. Barta-Schreiber, T. G. Langdon and H. Mughrabi: Ed. by M. J. Zehetbauer and R. Z. Valiev, Proceedings of 2nd international conference on nanomaterials by severe plastic deformation, (Weinheim, Wiley VCH, 2004) 677-683.

[60] J. D. Morrow: ASTM STP **378** (1965) 45-87.

[61] R. W. Landgraf: ASTM STP **467** (1970) 3-36.

[62] H. W. Höppel, Z. Zhou, H. Mughrabi and R. Z. Valiev: Philos. Mag. A **82** (2002) 1781-1794.

[63] C. Xu, Q. Wang, M. Zheng, J. Li, M. Huang, Q. Jia, J. Zhu, L. Kunz and M. Buksa: Mater. Sci. Eng. A **475** (2008) 249-256.

[64] Y. Furukawa, T. Fujii, S. Onaka and M. Kato: Mater. Trans. **50** (2009) 70-75.

[65] A. Vinogradov, Y. Kaneko, K. Kitagawa, S. Hashimoto, V. Stolyarov and R. Valiev: Scr. Mater. **36** (1997) 1345-1351.

[66] A. Vinogradov, Y. Kaneko, K. Kitagawa, S. Hashimoto and R. Valiev: Mater. Sci. Forum **269-272** (1998) 987-992.

[67] M. Goto, S. Z. Han, T. Yakushiji, C. Y. Lim and S. S. Kim: Scr. Mater. **54** (2006) 2101-2106.

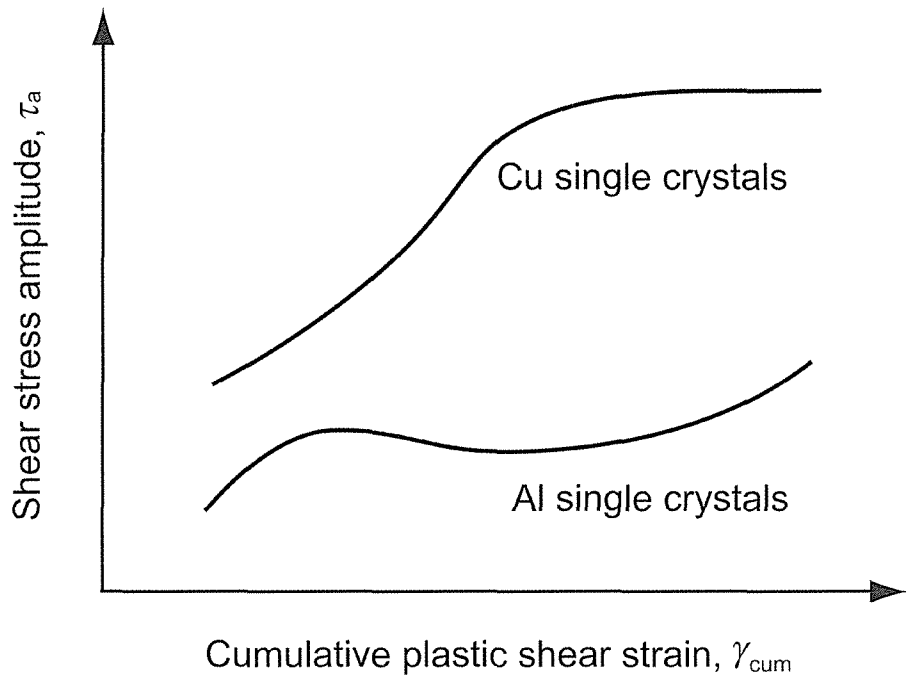

Figure 2-1. Schematic illustration of cyclic hardening/softening curves of Cu and Al single crystals obtained by the strain-controlled fatigue tests.

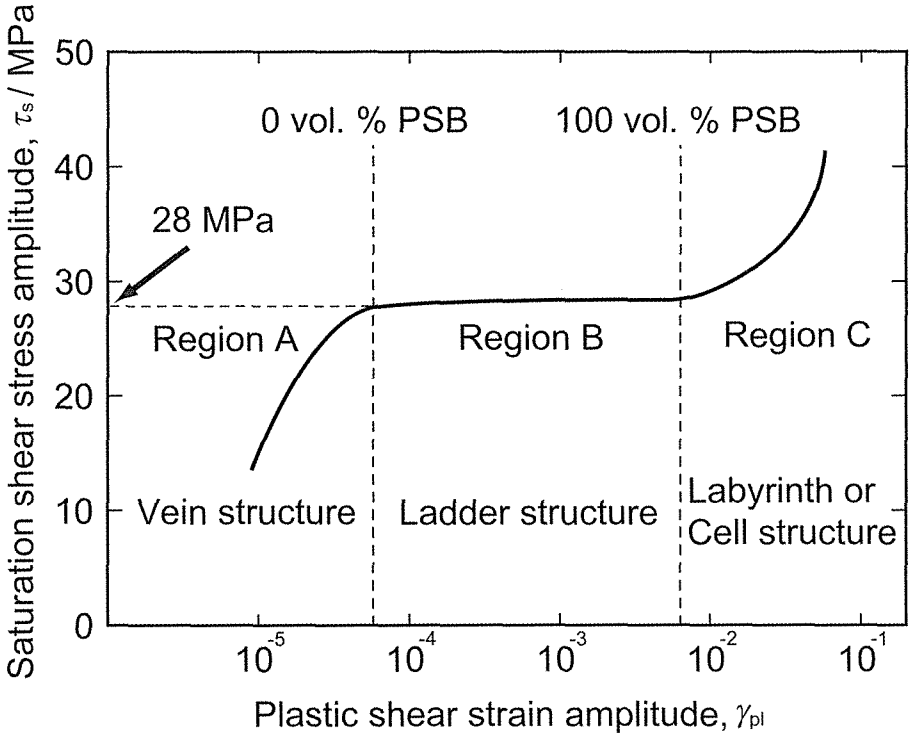

Figure 2-2. Cyclic stress-strain curve of Cu single crystals oriented for single slip fatigued at room temperature.

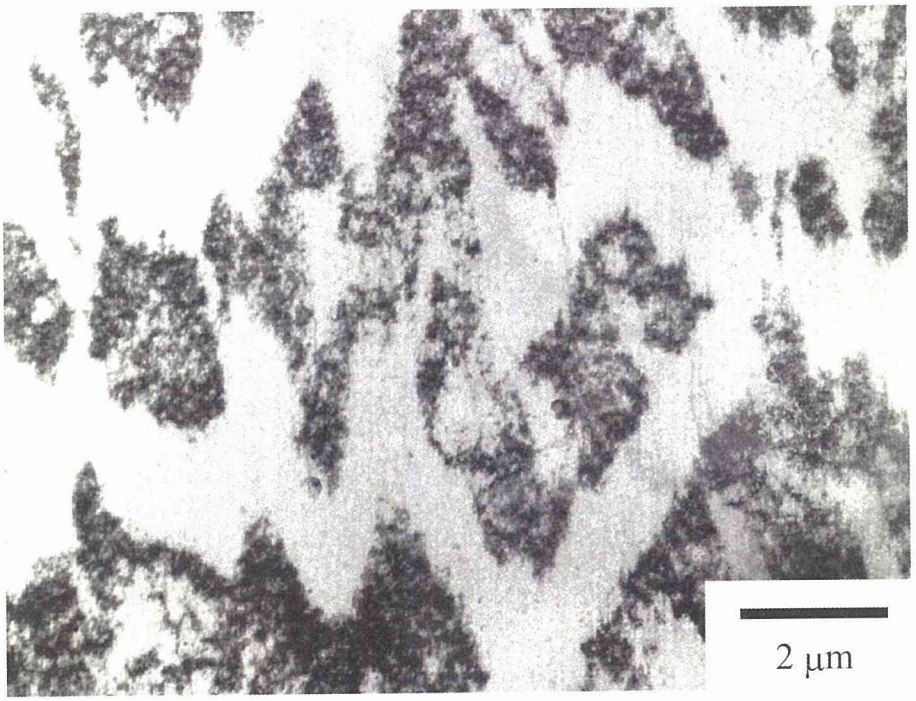

Figure 2-3. TEM image of vein structure in a Cu single crystal [13].

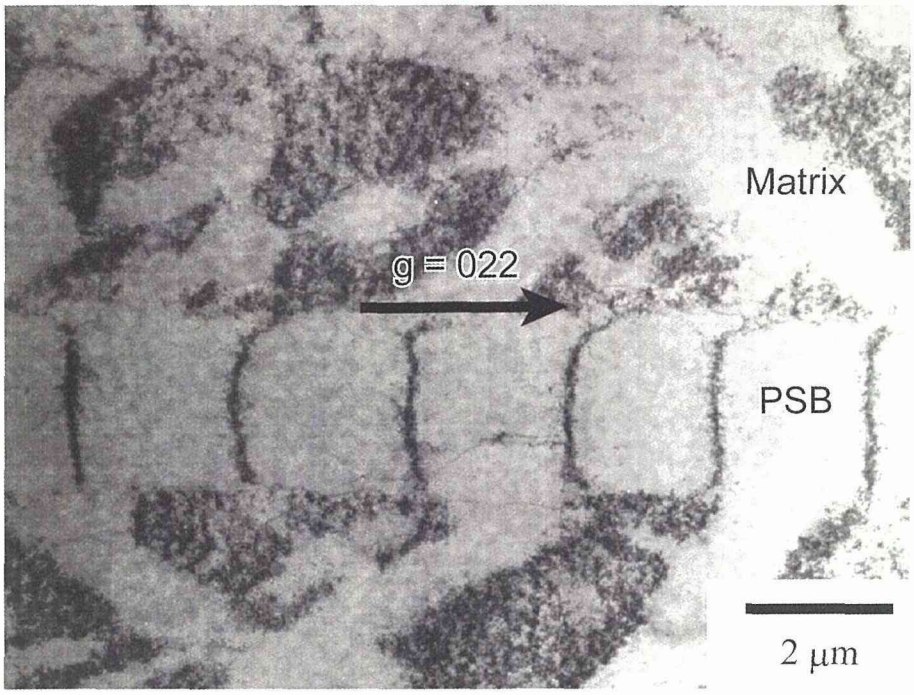

Figure 2-4. A transmission electron micrograph of the matrix vein and PSB ladder structures in a Cu single crystal. The PSB ladder walls are perpendicular to the primary slip direction [13].

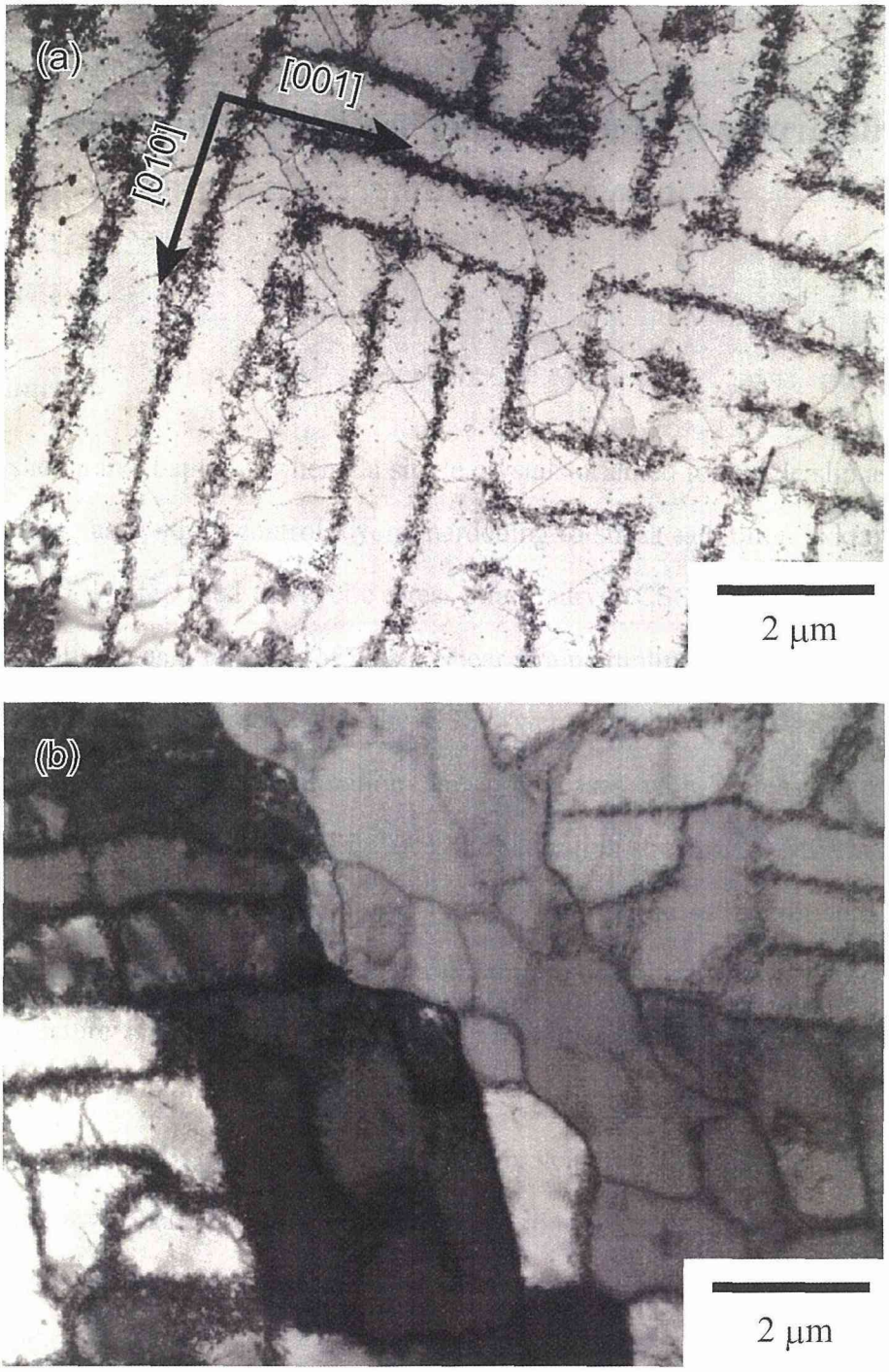

Figure 2-5. (a) Labyrinth structure formed in a 3003 Al alloy. The dislocation walls are parallel to the (001) and (010) planes. (b) Dislocation cell structure in a specimen of Cu single crystal. [13]

Chapter 3
Low-temperature cyclic deformation and microstructure of single-crystalline aluminum

3.1 Introduction

As shown in Chapter 2, when Cu single crystals oriented for single slip are cyclically deformed under plastic strain control, cyclic hardening to stress saturation is known to occur [1-6]. Mughrabi [1] reported the cyclic stress-strain curve (CSSC), a plot of the saturation shear stress amplitude as a function of plastic shear strain amplitude γ_{pl}, of Cu single crystals oriented for single slip and found that the CSSC were clearly divided into three regions: region A ($\gamma_{pl} < 6.5\times10^{-5}$); the saturation stress increases with increasing plastic strain amplitude, region B ($6.5\times10^{-5} \leq \gamma_{pl} \leq 7.5\times10^{-3}$); the saturation stress of 28 MPa is independent of the plastic strain amplitude and region C ($\gamma_{pl} > 7.5\times10^{-3}$); the saturation stress amplitude increases again with increasing the plastic strain amplitude. It is known that characteristic dislocation structure is formed in each region. In region A, the matrix vein structure is formed [1-4, 7]. In region B, deformation becomes inhomogeneous and the so-called persistent slip bands (PSBs) are formed. The matrix vein and PSB ladder structures [2-6, 8, 9] coexist and convey certain amounts of plastic strain amplitude. The PSBs convey much higher plastic strain than the matrix and the volume fraction of PSBs increases with increasing the plastic strain amplitude [9, 10]. In region C, the secondary slip systems become active and labyrinth and cell structures are formed [3, 7, 8].

Though the cyclic deformation behavior of Cu has been widely studied, there are only a few papers on cyclic deformation behavior of pure Al. Al single crystals oriented for single and multi slips show initial hardening followed by softening and secondary hardening

at room temperature [11-15]. For Al single crystals oriented for the $[\bar{1}23]$ stress direction, neither stress saturation nor PSB ladder structure is observed at room temperature [11], while Cu single crystals oriented for the same stress direction shows stress saturation and the formation of the PSB ladder structure [3].

The differences in cyclic deformation behavior and microstructure at room temperature between Cu and Al have been explained by considering the difference in stacking fault energy (SFE), reported values being 41 mJ/m^2 for pure Cu [16] and 122 mJ/m^2 for pure Al [17], and homologous temperature, T/T_m where T and T_m are the test temperature and melting point, respectively. Al-Mg solid-solution alloys with Mg contents from 0.6 to 0.7 mass % with SFE of 110 mJ/m^2 [18] show stress saturation [19, 20], stress plateau in CSSC [20] and the ladder structure [20] at room temperature. Moreover, Vorren and Ryum [21] reported that Al single crystals fatigued at 77 K under constant plastic strain amplitude showed stress saturation. In order to obtain comprehensive understanding of the fatigue mechanism for fcc metals, it is necessary to investigate the effects of SFE and homologous temperature on cyclic deformation behavior and microstructural development.

In the present study, low-cycle fatigue tests of pure Al single crystals oriented for single slip are carried out at 77 K. From the results of fatigue tests as well as surface and microstructural observation, the effects of SFE and test temperature on cyclic deformation behavior and microstructural development for Al single crystals will be investigated.

3.2 Experimental procedure

Al single crystals were grown by the Bridgman method from plates of 99.98 mass % Al. The single crystals were cut into specimens for fatigue tests with the gauge dimensions of 4×6×10 mm^3 by spark erosion so that the stress axis becomes parallel to the [419] direction. Figure 3-1 shows the stereographic projection indicating the stress axis, the slip systems and the Schmid factor (S. F.) of each slip system. The specimens with the $[21\bar{1}]$

surface normal were mechanically polished with silicon-carbide paper and electrolytically polished using solution of 20 % perchloric acid and 80 % methanol.

Fully reversed tension-compression low-cycle fatigue tests were carried out at 77 K for the single crystals under constant plastic shear strain amplitudes γ_{pl} in the range of 1×10^{-3} and 5×10^{-2} using an electro-hydraulic testing machine (Shimadzu Servo Pulser). The specimens were immersed in liquid nitrogen to achieve the low temperature atmosphere during the fatigue tests. Strain was measured with an extensometer mounted directly on the gauge section and constant strain rate of 2.34×10^{-3} s^{-1} was employed using a triangular command signal. After the shear stress amplitude saturated, the fatigue tests were stopped and the specimen surface was observed on an optical microscope (Nikon Optiphot).

The fatigued specimens were sliced into 3 mm disks parallel to the $(2\bar{1}1)$ plane and were ground down to a thickness of 0.2 mm with silicon-carbide paper. Then, the samples were electrolytically polished on a twin-jet polisher (Struers Tenupol-5) in solution of 8 % perchloric acid, 10 % 2-butoxyethanol and 82 % methanol. Microstructural observations were performed by using TEM (JEOL JEM 2011) with an acceleration voltage of 200 kV.

During the course of this study, it was found that when specimens fatigued at 77 K were left at room temperature, dislocation structure formed by the fatigue test disappeared within a few months. To avoid such possibility of natural annealing and to ensure the preservation of dislocation structure until TEM observation, fatigued specimens were always stored in liquid nitrogen.

3.3 Results

3.3.1 Cyclic deformation behavior of Al single crystals

Figure 3-2 shows the cyclic hardening curves of Al single crystals fatigued at 77 K with various γ_{pl}. The shear stress amplitude τ_a was plotted against cumulative plastic shear strain defined as

$$\gamma_{cum} = 4N\gamma_{pl} \quad (3\text{-}1)$$

where N is the number of fatigue cycles. It can be seen from Fig. 3-2 that all specimens show cyclic hardening to saturation. The saturation stress amplitude and corresponding cumulative strain amplitude are summarized in Table 3-1. When the plastic shear strain amplitude is in the range 2×10^{-3} to 1×10^{-2}, the saturation shear stress is almost independent of the plastic shear strain, staying close to 43 MPa. At higher strain amplitudes ($\gamma_{pl} \geq 3\times10^{-2}$), the saturation stress amplitude increases again with increasing the plastic shear strain amplitude. The CSSC is drawn in Fig. 3-3 by using the obtained saturation shear stresses and the results given by Vorren and Ryum [21] are also included. The CSSC shows a clear stress plateau in a range of plastic shear stress amplitude from 2×10^{-3} to 2×10^{-2}. Therefore, the CSSC of pure Al at 77 K can also be divided into three regions: region A ($\gamma_{pl} < 2\times10^{-3}$), region B ($2\times10^{-3} \leq \gamma_{pl} \leq 2\times10^{-2}$) and region C ($\gamma_{pl} > 2\times10^{-2}$), as the same way mentioned in Section 1.

3.3.2 Surface observation

The surface slip features of specimens fatigued at various plastic shear strain amplitudes are shown in Fig. 3-4 (a) to (c). These photographs were taken from $[21\bar{1}]$. In Fig. 3-4 (a), *i.e.*, in region A of Fig. 3-3, the traces of the primary slip plane are uniquely observed. On the other hand, in Fig. 3-4 (b) and (c) (region B of Fig. 3-3), primary, critical and conjugate slip traces are observed on the surface of the fatigued specimens. The activation of the critical and conjugate systems in region B is in contrast to the case of Cu single crystals where only the primary slip system is operative [1-3, 6, 9]. This remarkable and interesting point will be discussed in the following section.

3.3.3 Microstructural observation

The dislocation structure in the PSBs and in the matrix of a specimen fatigued at $\gamma_{pl} = 3\times10^{-3}$ are shown in Fig. 3-5 (a) and (b), respectively. The crystal orientation in Fig. 3-5 (a)

coincides with that in Figure 3-1. The PSB is formed parallel to the $(1\bar{1}1)$ primary slip plane as shown in Fig. 3-5 (a). From trace analysis, the dislocation walls in the PSB are found to be parallel to the (001) and (010) planes. For the PSB ladder structure formed in Cu single crystals, dislocation walls are usually parallel to the (011) plane [2-8, 27], *i.e.* perpendicular to the primary slip direction. Therefore the dislocation walls observed in this study have different geometry from that of the traditional ladder structure. It has been known that the labyrinth structure, consisting of two mutually perpendicular {100} dislocation walls, is formed by the activation of the primary and critical slip systems [22, 23]. As can be seen in Figure 3-1, for the [419] single crystals, the S. F. of the critical slip system $(111)[01\bar{1}]$ is 0.47. The activation of the critical slip system is, therefore, quite easy. As shown in Figure 3-4, the primary and critical slip traces were indeed observed in the specimen fatigued with γ_{pl} within the plateau region. After all, the observed dislocation structure in Figure 3-5 (a) can be reasonably characterized as the labyrinth structure.

Figure 3-5 (b) shows the microstructure of the matrix (outside of PSBs) in a specimen fatigued at $\gamma_{pl} = 3\times10^{-3}$. The dislocations in the observed vein structure align approximately parallel to the (001) and (010) planes. Though the vein structure parallel to {100} is found in fatigued Cu single crystals with the [001] stress axis [22, 24], as far as the authors know, such vein structure has not been observed in Cu single crystals oriented for single slip. Therefore, for [419] Al single crystals fatigued at plastic shear strain amplitude in region B, it is expected that multiple slip systems, *i.e.* the primary, critical and conjugate slip systems, are active and {100} dislocation walls start developing even in the matrix.

3.4 Discussion

3.4.1 Dependence of the channel width on shear stress amplitude

For Cu single crystals, the PSB ladder structure is generally softer than the matrix vein structure. Once the PSBs are formed, the PSBs preferentially convey applied plastic

strain. The volume fraction of the PSBs increases with increasing plastic strain amplitude within the plateau region (region B) [9, 10]. Since the PSB ladder structure itself is unchanged during cyclic deformation in the plateau region, the plateau stress can be quantitatively explained by the flow stress of the PSBs.

If the PSBs formed in Al at 77 K act in the same manner as those formed in Cu at room temperature, the stress amplitude should be determined by the flow stress of the PSBs. In this section, let us discuss whether the PSBs formed in Al dominantly convey applied plastic strain or not by considering channel width between adjacent {100} dislocation walls and stress amplitude in region B.

Basinski *et. al.* [2] have reported that there is a linear relationship between the shear stress amplitude τ_a and the reciprocal of the channel width $1/d_c$, *i. e.*,

$$\tau_a = \frac{\alpha \mu b}{d_c} \tag{3-2}$$

where α is a dimensionless constant to be determined, μ the shear modulus and b the magnitude of the Burgers vector. Though Brown [25, 26], Mughrabi and Pschenitzka [27] proposed more detailed relationships, eq. (3-2) is adopted here not only for simplicity but also for different geometry: the {100} walls of the labyrinth structure observed in the present study are different from the usual {110} walls of the ladder structure in fcc metals. With μ = 26.7 GPa and b = 0.286 nm, obtained values of the constant α are between 2.1 and 2.3 (see Table 3-2). According to theoretical studies by Brown [25] and Pedersen [28, 29], α is estimated to be 2.0. Therefore, the present values of α are in agreement with the theoretical one.

Figure 3-6 plots the shear stress amplitude as a function of the reciprocal channel width. The results of Al single crystals fatigued at room temperature [12, 30] are also included in Fig. 3-6. From the slope of the straight line, α = 2.2 is obtained, again in agreement with the theoretically estimated value. It is now clear that the plateau stress is explained by the flow stress of the PSBs containing the {100} dislocation walls and the PSBs in Al do convey applied plastic strain. Therefore, it is expected that the volume fraction of

PSBs should increase with increasing plastic strain amplitude in region B.

3.4.2 Effects of test temperature, stress direction and SFE on cyclic deformation behavior

In this study, cyclic deformation behavior and dislocation structure of Al single crystals at 77 K were quite different from those at room temperature [11-15]. Many investigators reported that test temperature affects cyclic deformation behavior and microstructural development of Cu [31-33] and Ni [5, 34-36]. Lisiecki and Weertman [32, 33] reported that Cu single crystals show the stress plateau in the CSSC at 523 K (T/T_m = 0.39) and no stress plateau at 678 K (T/T_m = 0.50). Although Ni single crystals show the stress plateau in a range of test temperatures from 77 K (T/T_m = 0.04) to 750 K (T/T_m = 0.41), the width of the stress plateau becomes narrower with increasing test temperature [34-36]. In terms of the homologous temperature, room temperature for Al (T/T_m = 0.32) is higher than that for Cu (T/T_m = 0.22) and Ni (T/T_m = 0.17). Judging from the above experimental results, it is very likely that the higher homologous temperature causes the absence of the stress plateau when Al single crystals are fatigued at room temperature. On the other hand, since 77 K is low enough even for Al, monotonic cyclic hardening to saturation and the stress plateau were observed in the present study. Therefore, test temperature plays an important role on the cyclic deformation behavior of Al single crystals.

Microstructure observed in the PSBs for Al single crystals fatigued at 77 K was different from that for Cu single crystals fatigued at room temperature. The noteworthy point is that the secondary slip system was active in the PSBs in region B. Since the PSBs are formed parallel to the primary slip plane, only the primary slip system must have been activated at the initial stages of the fatigue tests. If the secondary slip system becomes operative as increasing fatigue cycles, the formation of the labyrinth structure in the PSBs can be understood reasonably.

Why do the multiple slip systems become active in the Al PSBs? There are two possible factors, stress direction and high SFE of Al. As described in Section 3.3, the critical

slip system $(111)[01\bar{1}]$ is easily activated in the [419] single crystals of fcc metals. However, for single-crystalline Cu [6] and Al-0.7 mass % Mg [20] oriented to [419], only {110} walls of the ladder structure are formed in the PSBs fatigued at room temperature in region B. Therefore, the easy occurrence of the secondary slip system in Al cannot be explained merely in term of the stress direction.

We believe that the origin of the notable difference among Cu, Al-0.7 mass % Mg and Al in the microstructural development can be found in the SFE values. The SFE of pure Al is reported to be 122 mJ/m^2 [17] and these are higher than those of pure Cu (41 mJ/m^2 [16]) and Al-0.6 mass % Mg (110 mJ/m^2 [18]). The higher SFE and, thus, the smaller width of extended dislocations in Al make an activation of the secondary slip easier and resultantly the labyrinth structure is developed in PSBs even at 77 K. Therefore, SFE plays an important role in the microstructural development of Al even at 77 K. We conclude that, in addition to temperature, the SFE is also a key factor in understanding the cyclic deformation behavior and dislocation microstructure of pure Al single crystals.

3.5 Conclusions

Low-cycle plastic-strain-controlled fatigue tests of [419] single slip oriented Al single crystals were carried out at 77 K. The results and conclusions are summarized as follows.

(1) During strain-controlled fatigue tests at 77 K, Al single crystals show monotonic hardening to stress saturation at all the tested strain amplitudes. The CSSC shows a stress plateau with the stress amplitude of 43 MPa in a range of plastic shear strain amplitude from 2×10^{-3} to 2×10^{-2}.

(2) The PSBs are formed parallel to the primary slip planes during cyclic deformation at 77 K. In the PSBs, well-developed {100} walls are formed by the activation of multiple slip systems, *i.e.* the primary and critical slip systems.

(3) Good correlation can be found between reciprocal of the channel width of the dislocation walls and the saturation stress. Therefore, it is expected that PSBs carry the applied plastic strain and their volume fraction increase with increasing plastic strain amplitude.

(4) Both temperature and SFE play important roles in the cyclic deformation behavior and the microstructural development of pure Al single crystals: the existence of the stress plateau can be explained by the temperature effect and the occurrence of the multiple slip systems and the formation of two {100} dislocation walls can be explained by the SFE effect.

References

[1] H. Mughrabi: Mater. Sci. Eng. **33** (1978) 207-223.

[2] Z. S. Basinski, A. S. Korbel and S. J. Basinski: Acta Metall. **28** (1980) 191-207.

[3] N. Y. Jin: Acta. Metall. **37** (1989) 2055-2066.

[4] U. Holzwarth and U. Essmann: Appl. Phys. A **58** (1994) 197-210.

[5] J. Bretschneider, C. Holste and W. Kleinert: Mater. Sci. Eng. A **191** (1995) 61-72.

[6] C. Watanabe, K. Kanmuri, M. Kato, S. Onaka and T. Fujii: Philos. Mag. A **82** (2002) 855-866.

[7] C. Laird: Mater. Sci. Eng. **81** (1986) 433-450.

[8] F. Ackermann, L. P. Kubin, J. Lepinoux and H. Mughrabi: Acta. Metall. **32** (1984)715-725.

[9] P. Lukáš and L. Kunz: Philos. Mag. **84** (2004) 317-330.

[10] A. T. Winter: Philos. Mag. **30** (1974) 719-738.

[11] O. Vorren and N. Ryum: Acta Metall. **36** (1988) 1443-1453.

[12] M. Videm and N. Ryum: Mater. Sci. Eng. A **219** (1996) 1-10.

[13] J. Wang, Z. G. Zhu, Q. F. Fang and G. D. Liu: Mater. Res. Bull. **34** (1999) 1729-1739.

[14] T. Fujii, N. Sawatari, S. Onaka and M. Kato: Mater. Sci. Eng. A **387-389** (2004) 486-490.

[15] P. Li, S. Li, Z. Wang and Z. Zhang: Metall. Mater. Trans. A **41** (2010) 2532-2537.

[16] D. J. H. Cockayne, M. L. Jenkins and I. L. F. Ray: Philos. Mag. **24** (1974) 1383-1392.

[17] V. Yamakov, D. Wolf, M. Salazar, S. R. Phillpot and H. Gleiter: Acta Mater. **49** (2001) 2713-2722.

[18] S. Kritzinger, P. S. Dobson and R. E. Smallman: Philos. Mag. **16** (1967) 217-229.

[19] B. Ramaswami and T. W. F. Lau: Mater. Sci. Eng. **46** (1980) 221-230.

[20] T. Fujii, S. Uju, C. Watanabe, S. Onaka and M. Kato: Mater. Sci. Forum **561-565** (2007) 2213-16.

[21] O. Vorren and N. Ryum: Acta Metall. **35** (1987) 855-866.

[22] P. Li, S. X. Li, Z. G. Wang and Z. F. Zhang: Acta Mater. **58** (2010) 3281-3294.

[23] N. Y. Jin and A. T. Winter: Acta Metall. **32** (1984) 989-995.

[24] Z. Wang, B. Gong and Wang: Acta Mater. **45** (1997) 1379-1391.

[25] L. M. Brown: Mater. Sci. Eng. A **285** (2000) 35-42.

[26] L. M. Brown: Philos. Mag. **86** (2006) 4055-4068.

[27] H. Mughrabi and F. Pschenitzka: Philos. Mag. **85** (2005) 3029-3045.

[28] O. B. Pedersen: Acta. Metall. **38** (1990) 1221-1239.

[29] O. B. Pedersen: Philos. Mag. **73** (1996) 829-858.

[30] T. Fujii, S. Uju, H. Tanaka, T. Murayama, C. Watanabe, S. Onaka and M. Kato: Plasticity, Failure and Fatigue in Structural Materials from Macro to Nano, Proc. of the Hael Mughrabi Honorary Symposium, Eds., K. J. Hsia,M.Göken, T. Pollock, P. D. Portella and N. R. Moody, The Minerals, Metals & Material Society, 2008, 123-127.

[31] H. Shirai and J. R. Weertman: Scr. Metall. **17** (1983) 1253-1258.

[32] L. L. Lisiecki and J. R. Weertman: Scr. Metall. **20** (1986) 249-252.

[33] L. L. Lisiecki and J. R. Weertman: Acta Metall. **38** (1990) 509-519.

[34] J. Bretschneider, C. Holste and B. Tippelt: Acta Mater. **45** (1997) 3775-3783.

[35] M. Hollmann, J. Bretschneider and C. Holste: Cryst. Res. Technol. **35** (2000) 479-492.

[36] C. Holste: Philos. Mag. **84** (2004) 299-315.

Table 3-1. Experimental values of cumulative plastic shear strain γ_{cum} and saturation shear stress amplitude τ_s for Al single crystals.

Plastic shear strain amplitude, γ_{pl}	Cumulative plastic shear strain, γ_{cum}	Saturation shear stress amplitude, τ_s [MPa]
1×10^{-3}	40.0	24.3
2×10^{-3}	68.0	45.0
3×10^{-3}	96.0	44.5
5×10^{-3}	100.6	43.7
7×10^{-3}	84.0	41.7
1×10^{-2}	80.0	42.4
3×10^{-2}	91.8	50.8
5×10^{-2}	25.6	53.8

Table 3-2. Experimental values of saturation stress amplitude τ_a, channel width d_c and calculated values of constant α for Al single crystals.

Plastic shear strain amplitude, γ_{pl}	Saturation shear stress amplitude, τ_a [MPa]	Channel width, d_c [nm]	Dimensionless constant, α
3×10^{-3}	44.5	390	2.3
5×10^{-3}	43.7	370	2.2
7×10^{-3}	41.7	400	2.1
1×10^{-2}	42.4	430	2.2

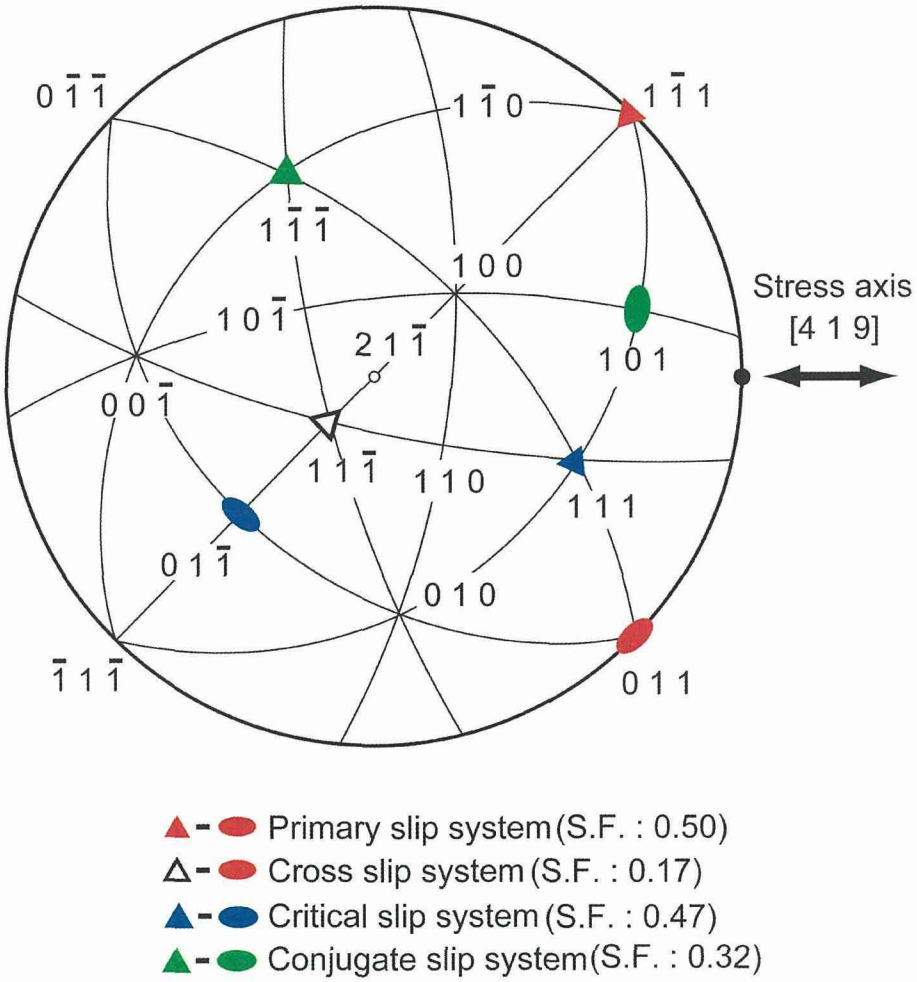

Figure 3-1. Stereographic projection indicating the stress-axis orientation, the slip systems and the Schmid factor (S. F.) of each slip system.

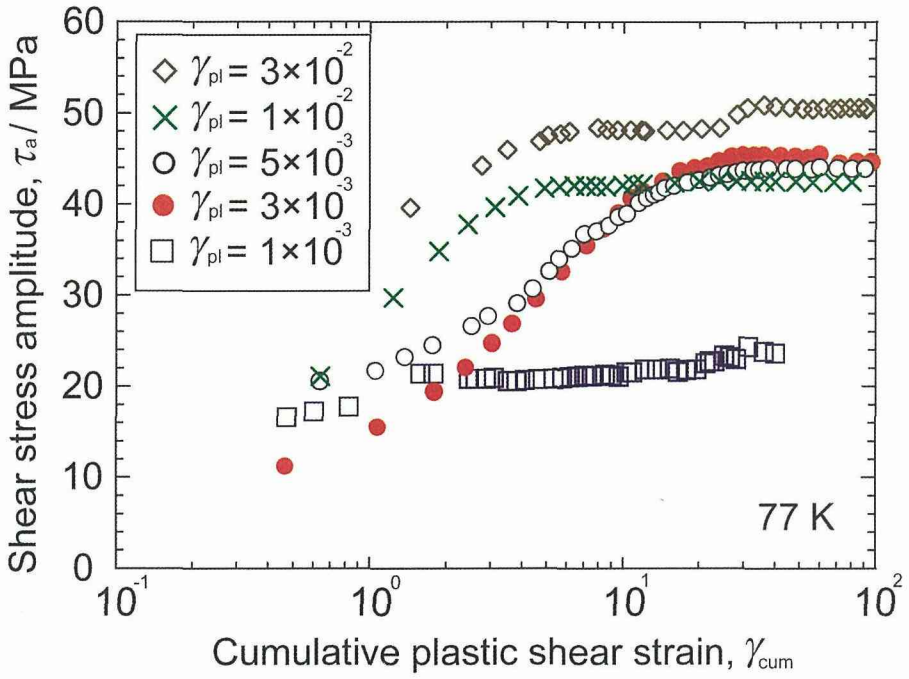

Figure 3-2. Cyclic hardening curves of Al single crystals fatigued at 77 K with various plastic strain amplitudes.

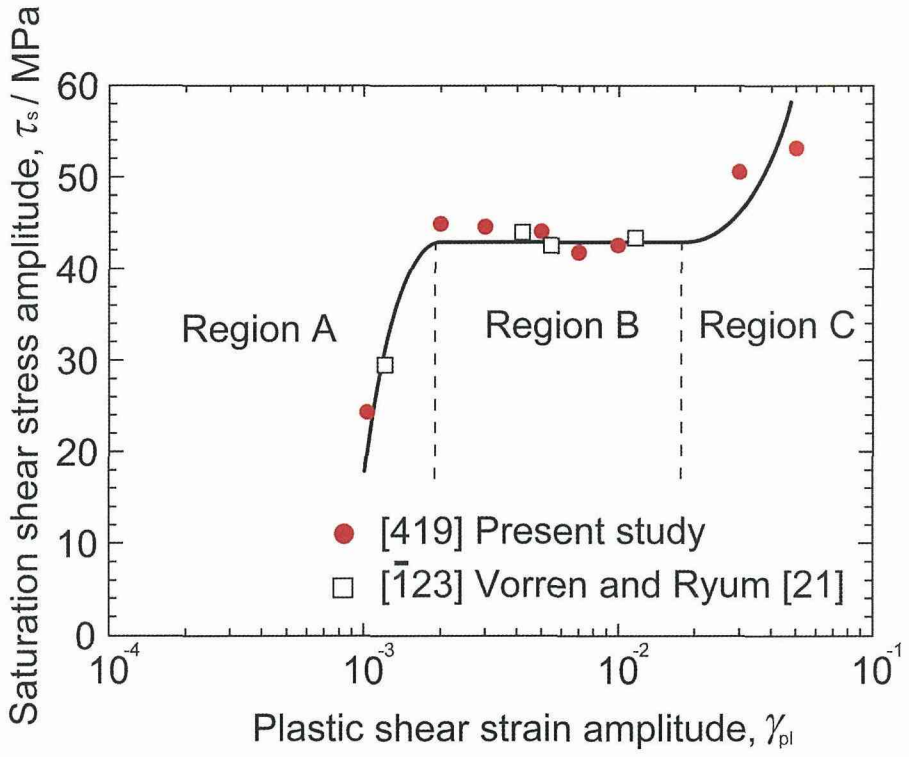

Figure 3-3. Cyclic stress-strain curve of single-crystalline Al fatigued at various plastic shear strain amplitudes at 77 K. Experimental data obtained by Vorren and Ryum [21] are also plotted.

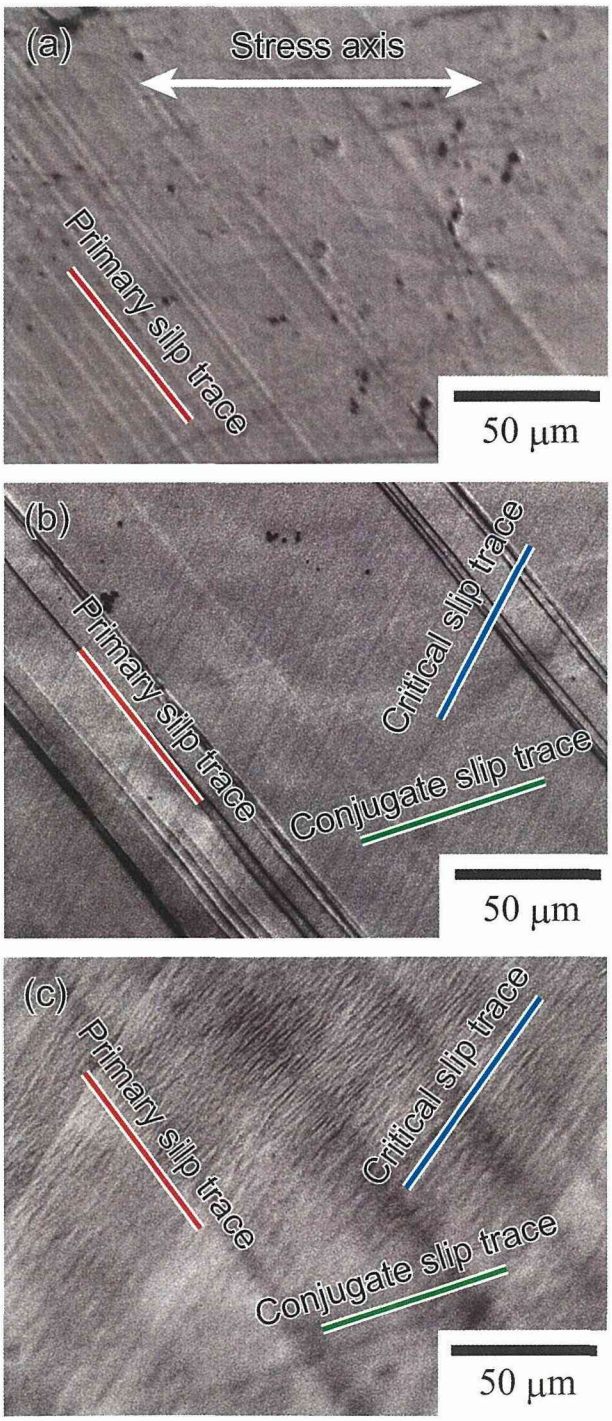

Figure 3-4. Optical micrographs taken from $(21\bar{1})$ plane of a specimen fatigued at (a) $\gamma_{pl} = 1\times10^{-3}$ until $\gamma_{cum} = 40$, (b) $\gamma_{pl} = 3\times10^{-3}$ until $\gamma_{cum} = 96$, (c) $\gamma_{pl} = 1\times10^{-2}$ until $\gamma_{cum} = 80$.

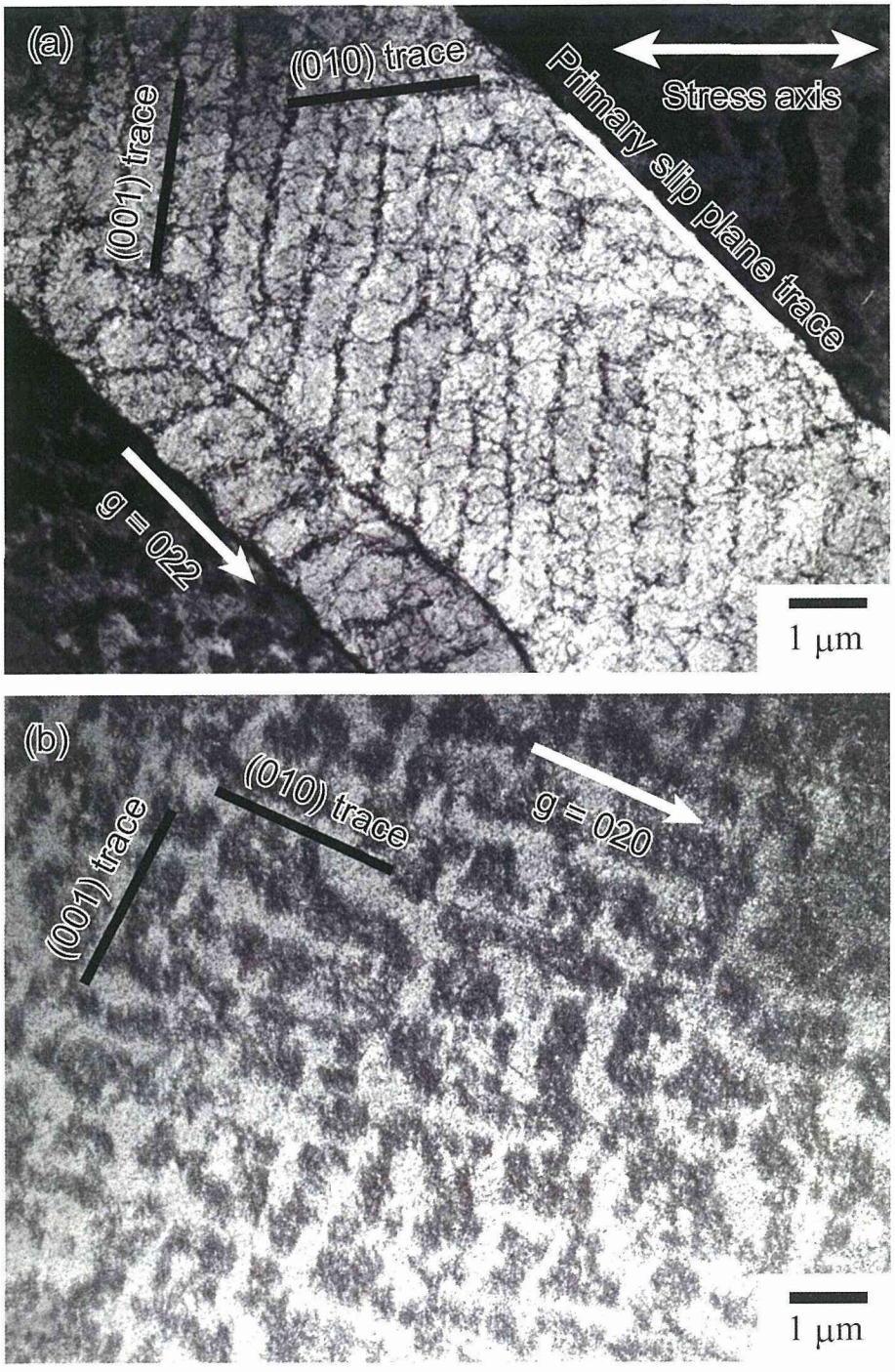

Figure 3-5. (a) Well-developed dislocation walls in PSB of a specimen fatigued at $\gamma_{pl} = 3\times10^{-3}$ until $\gamma_{cum} = 96$ at 77 K. Zone axis: $[21\bar{1}]$, (b) Matrix vein structure in the same specimen as in (a) but in the different area. Zone axis: [100].

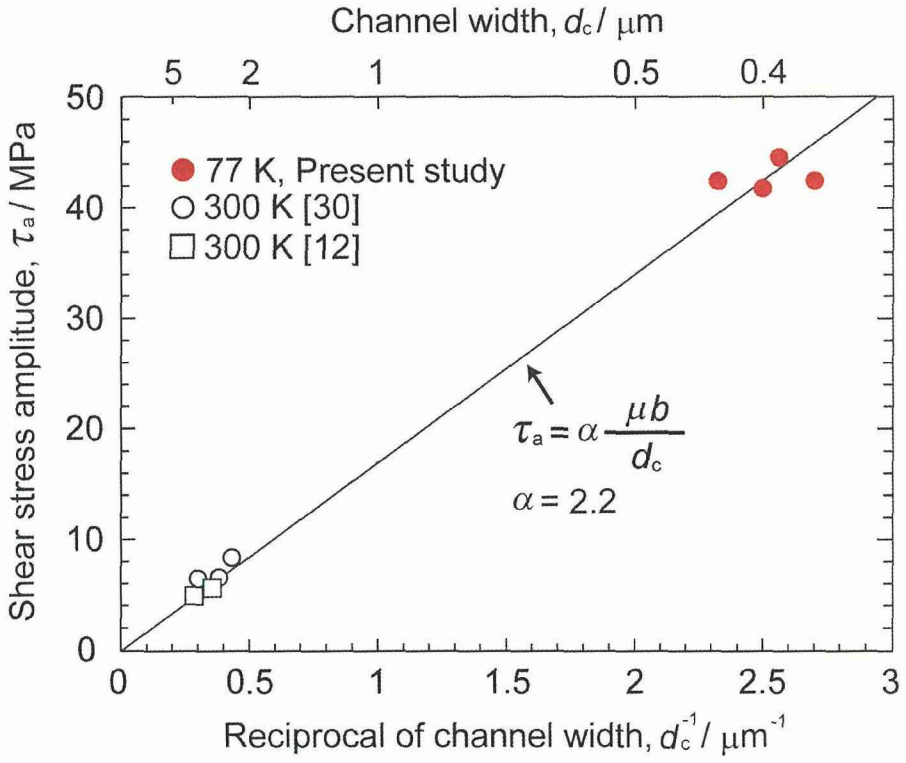

Figure 3-6. Relationship between shear stress amplitude τ_a and reciprocal of channel width $1/d_c$. Experimental data for single-crystalline Al fatigued at 77 K [12, 30] are also plotted.

Chapter 4
Low-temperature cyclic deformation and microstructure of ultrafine-grained aluminum

4.1 Introduction

Cyclic deformation behavior of ultrafine-grained (UFG) fcc metals is known to show some characteristic features such as cyclic softening [1-5], formation of local shear bands [1, 3-7] and local grain coarsening [1, 2, 5, 8, 9]. Though there are many studies on mechanical and physical properties of UFG materials, the reason why UFG metals show such cyclic deformation characteristics has not been well understood. Using UFG Cu, Höppel *et al.* [2] reported that the amount of cyclic softening and grain coarsening during cyclic deformation became less significant at 223 K compared to those at 293 K. Thiele *et al.* [10] showed similar results for UFG Ni. Therefore, it is suggested that test temperature is an important factor to affect cyclic deformation behavior and microstructural development of UFG materials.

In this study, low-cycle strain-controlled fatigue tests were carried out under plastic strain control at various temperatures between 300 K and 83 K using UFG pure Al fabricated by an equal channel angular pressing (ECAP) technique. From the results of the fatigue tests as well as scanning electron microscope (SEM) and transmission electron microscope (TEM) observations, the effects of test temperature on cyclic deformation behavior and microstrucural changes of UFG Al will be examined.

4.2 Experimental procedure

4.2.1 Equal channel angular pressing

In this study, the ECAP method, one of the severe plastic deformation processes, was used for production of UFG Al. Figure 4-1 shows the principle of the ECAP process. The ECAP tool is a die with two intersecting channels of identical cross-section. At first, a sample is put into the top of the die and pressed forcibly. When a sample is pressed through the bending section, shear strain is introduced. Since sample sectional area does not change thorough single pass, the above pass can be repeated many times and the ECAP process can produce large plastic strain to samples.

During the repeated pressing process, three different routes are typically used; route A: this process denotes repetitive pressing without rotation of sample, route B_C: for this sequence of pressings, the sample is rotated by 90° between each pressing and route C: the sample is rotated thorough 180° between each pressing [11, 12]. Among these, route B_C is known to be more effective than the other two routes for producing equiaxed grain structure [12, 13].

4.2.2 Specimen preparation

High-purity Al (99.98 ~ 99.99 mass %) sheets were annealed at 673 K for 2 h and then cut to the rod shape with 10 mm in diameter and 60 mm in length. The rod samples were subjected to the ECAP process. The ECAP process was conducted at room temperature with a pressing speed of 16 mm s^{-1} and each rod is coated in a MoS_2 lubricant. Each rod was subjected to 8 passes of ECAP under route B_C [12, 13]. It is known that there are essentially no changes in the average grain size when the pressing is continued after 8 passes [14, 15]. After the ECAP deformation, average grain size became about 1.3 μm. According to Salem *et al.* [16], grain refinement in pure Al is strongly dependent on the purity of the material. In fact, Kawasaki *et al.* has reported that the grain size of 99.99 mass % Al can be at the smallest 1.2 μm by the ECAP technique [15]. Therefore, the obtained average

grain size of 1.3 μm in the present study is reasonably larger than that of commercially pure Al fabricated by the same ECAP condition [17, 18]. Nevertheless, high purity Al has been chosen for the purpose of avoiding the effects of impurities and investigating the primary mechanical and physical properties of Al.

4.2.3 Fatigue tests

The fatigue specimens with the gauge length of 10 mm and cross-sectional area of 4×6 mm^2, were taken from the central part of the ECAPed rods by spark erosion in the direction parallel to the rod axis. The specimens were mechanically polished with silicon-carbide paper and electrolytically polished using solution of 20 % perchloric acid and 80 % methanol.

Fully reversed tension-compression low-cycle fatigue tests were carried out under a constant plastic tensile strain amplitude of $\varepsilon_{pl} = 1\times10^{-3}$ at room temperature (300 K) and low temperatures (198 K, 148 K, 123 K and 83 K) using an electro-hydraulic testing machine (Shimadzu Servopet). Low temperature atmosphere was achieved using a liquid nitrogen injection apparatus. Temperature during the fatigue tests was controlled within ±5 K by adjusting the amount of liquid nitrogen flow in the apparatus. Strain was measured with an extensometer mounted directly on the gauge section and constant strain rate of 4×10^{-3} s^{-1} was employed using a triangular command signal. Fatigue tests were interrupted when cumulative plastic tensile strain ε_{cum} defined as

$$\varepsilon_{cum} = 4N\varepsilon_{pl} \tag{4-1}$$

reached 10, where N is the number of fatigue cycles and $\varepsilon_{pl} = 1\times10^{-3}$. After the fatigue tests, specimen surfaces were observed by using a JEOL 5310 SEM.

During the course of this study, it was found that when fatigued specimens at 77 K were stored at room temperature, dislocation structure formed in UFG Al by the fatigue test disappeared in a few weeks. To avoid such possibility of natural annealing and to ensure the preservation of dislocation structure until TEM observation, fatigued specimens were always

stored in liquid nitrogen.

4.2.4 Microstructural observation

The fatigued specimens were sliced into 3 mm diameter disks and ground down to a thickness of 0.2 mm using silicon-carbide paper. Then, the samples were electrolytically polished using a twin-jet polisher (Struers Tenupol-5) in solution of 8 % perchloric acid, 10 % 2-butoxyethanol and 82 % methanol. Microstructure observations were performed by using a JEOL 2011 TEM at an acceleration voltage of 200 kV.

4.3 Results and discussion

4.3.1 Cyclic hardening and softening

Figure 4-2 shows cyclic hardening/softening curves of UFG Al tested at various temperatures. At 300 K, UFG Al shows hardening followed by rapid cyclic softening. Since macroscopically-visible cracks were formed on the specimen surface, the fatigue test at 300 K was stopped well before cumulative plastic tensile strain reached $\varepsilon_{cum} = 10$. It can be seen from Fig. 4-2 that with decreasing test temperature, tensile stress amplitude becomes larger and cyclic softening becomes less significant. At 83 K, UFG Al shows slight hardening followed by near saturation, *i.e.*, tensile stress amplitude $\sigma_a = 155$ MPa does not change much with increasing fatigue cycles after $\varepsilon_{cum} \approx 1$.

4.3.2 Shear band formation

Figures 4-3 (a) to (e) show a series of SEM images taken from specimens fatigued at various temperatures. Shear bands composed of intrusions and extrusions were formed on the surface of specimens. As can be seen, these shear bands extend over much larger distances than the average grain size of about 1.3 μm. In the previous study [4,5], it was found that strain localization occurred in the shear bands during cyclic deformation and

micro-cracks initiated along the shear bands. Similarly, micro-cracks are observed along the shear bands in the present study, as shown by the arrow in Fig. 4-3 (a). The area fraction and the length of the shear bands decrease with decreasing test temperature (Figs. 4-3 (b) to (e)). At 83 K, shear bands could not be detected on the specimen surface. Since the amount of cyclic softening becomes less with decreasing the fraction of shear bands, the formation of shear bands is considered to contribute to the cyclic softening of UFG Al.

4.3.3 Microstructural observation

The microstructures of an as-ECAPed specimen and a specimen fatigued at 300 K are shown in Figs. 4-4 (a) and (b), respectively. Comparison of Fig. 4-4 (a) with (b) reveals that grain growth has occurred to some extent even when the fatigue test was forced to be interrupted well before ε_{cum} reached 10 (See Fig. 4-2). On the other hand, no distinct dislocation substructure can be seen even in larger grains.

When test temperature decreases, microstructural changes during cyclic deformation become more noticeable, as shown in Fig. 4-5 to 4-8. At 198 K, in addition to local grain coarsening (Fig. 4-5), cell structure was formed in some coarsened grains (Fig. 4-6). With decreasing test temperature, the fraction of coarsened grains decreases and dislocation structures are formed even in smaller grains. For example at 83 K, primitive dislocation walls were formed in grains as small as 1.5 μm (Fig. 4-7 (a)) and well-developed dislocation walls were formed in larger grains (Figs. 4-7 (b) and (c)). Moreover, the fraction of grains that contain cell and wall structures increases with decreasing test temperature. Figure 4-8 shows that the fraction is nearly 50 % when fatigued at 83 K.

Average channel width between adjacent dislocation walls is about 300 nm and this value is much less than the frequently observed values between 1 to 4 μm in single-crystalline Al [19-22]. As shown in Figs. 4-7 (b) and (c), the dislocation walls appear to align parallel to the {100} plane just like those formed in single-crystalline and coarse-grained (CG) Al [19-23]. It is known that the multiple slip is responsible for the formation of the {100} walls and labyrinth structure in fcc metals [21, 24]. It is very probable that such multiple slip (or

the interaction between different slip systems) occurs very frequently in highly constrained grains of UFG materials. Therefore, it is expected that the wall structures in Figs. 4-7 (b) and (c) were formed in the same manner as those formed in single-crystalline and CG Al. This is the first observation of cell and wall structures in UFG Al after cyclic deformation. From the above experimental results, well-developed dislocation structures are formed only at low enough temperatures in UFG Al.

4.3.4 Dependence of the channel width on stress amplitude

In the present study, well-developed dislocation walls were observed at 83 K. It was found that the channel width of UFG Al was much smaller than that of single-crystalline and CG Al [19-22]. As shown in Chapter 3, the relationship between the shear stress amplitude τ_a and reciprocal of channel width between adjacent dislocation walls $1/d_c$ is described as [25]:

$$\tau_a = \frac{\alpha \mu b}{d_c} \tag{4-2}$$

where α is a dimensionless constant to be determined, μ the shear modulus and b the magnitude of the Burgers vector. Though Brown [26, 27] and Mughrabi and Pschenitzka [28] proposed more detailed relationships, eq. (4-2) is adopted not only for simplicity but also for different geometry: the <100> walls observed in the present study are different from the usual <110> walls of the so-called ladder structure in fcc metals [24, 29-31]

Converting the shear stress amplitude into tensile stress amplitude σ_a and using the Taylor factor $M = 3.06$, eq. (4-2) becomes

$$\sigma_a = \frac{\alpha M \mu b}{d_c} \tag{4-3}$$

With the experimental results of UFG Al fatigued at 83K, *i.e.*, σ_a = 155 MPa, d = 300 nm together with μ = 26.7 GPa and b = 0.286 nm, α = 1.9 is obtained from Eq. (4-3). This value of α is in good agreement with theoretically estimated value, 2.0 [26, 32-34].

Figure 4-9 summarizes the experimental results of the reciprocal of channel width under a given tensile stress amplitude for single-crystalline Al [21-23] and UFG Al in this study. As can be seen, all the data points lie on a single straight line. From the slope of the straight line, $\alpha = 2.1$ is obtained and this value is again reasonable. Therefore, the channel width of dislocation walls in UFG Al is also determined by the tensile stress amplitude in the same manner as that of single-crystalline and CG Al.

4.4 Conclusions

The low-cycle fatigue behavior of UFG Al was investigated under plastic strain control at various temperatures between 300 K and 83 K. It has become clear that test temperature plays an important role on the cyclic deformation behavior and formation of dislocation structures. The following conclusions have been obtained.

(1) With decreasing test temperature,
- Cyclic softening becomes less significant.
- Fraction of shear bands decreases.
- Fraction of coarsened grains decreases.
- Formation of dislocation cell and wall structures becomes easier.

(2) For UFG Al, good correlation can be found between reciprocal of the channel width of the dislocation walls and the saturation stress from single-crystalline Al and UFG Al. Therefore, the channel width of dislocation walls in UFG Al is also determined by the tensile stress amplitude in the same manner as that of single-crystalline and CG Al.

References

[1] S. R. Agnew and J. R. Weertman: Mater. Sci. Eng. A **244** (1998) 145-153.

[2] H. W. Höppel, Z. Zhou, H. Mughrabi and R. Z. Valiev: Philos. Mag. A **82** (2002) 1781-1794.

[3] L. Kunz, P. Lukáš and M. Svoboda: Mater. Sci. Eng. A **424** (2006) 97-104.

[4] C. Xu, Q. Wang, M. Zheng, J. Li, M. Huang, Q. Jia, J. Zhu, L. Kunz and M. Buksa: Mater. Sci. Eng. A **475** (2008) 249-256.

[5] Y. Furukawa, T. Fujii, S. Onaka and M. Kato: Mater. Trans. **50** (2009) 70-75.

[6] S. D. Wu, Z. G. Wang, C. B. Jiang, G. Y. Li, I. V. Alexandrov and R. Z. Valiev: Scr. Mater. **48** (2003) 1605-1609.

[7] M. Goto, S. Z. Han, T. Yakushiji, C. Y. Lim and S. S. Kim: Scr. Mater. **54** (2006) 2101-2106.

[8] H. Mughrabi and H. W. Höppel: Mat. Res. Sym. Proc. **634** (Erlangen, 2001) B2.2.1-B2.2.11.

[9] H. W. Höppel, M. Brunnbauer, H. Mughrabi, R. Z. Valiev and A. P. Zhilyaev: Proc. Materials Week 2000, (Wiley-VCH, 2001) http://www.materialsweek.org/ proceedings.

[10] E. Thiele, J. Bretschneider, L. Hollang, N. Schell and C. Holste: Investigations and Applications of Severe Plastic Deformation (2000) 173-178.

[11] Y. Iwahashi, M. Furukawa, Z. Horita, M. Nemoto and T. G. Langdon: Metall. Mater. Trans. **29** (1998) 2245-2252.

[12] Y. Iwahashi, M. Furukawa, Z. Horita, M. Nemoto and T. G. Langdon: Acta Mater. **46** (1998) 3317-3331.

[13] A. Mishra, V. Richard, F. Gregori, R. J. Asaro and M. A. Meyers: Mater. Sci. Eng. **410-411** (2005) 290-298.

[14] F. Dalla Torre, R. Lapovok, J. Sandlin, P. F. Thomson, C. H. J. Davies and E. V. Pereloma: Acta Mater. **52** (2004) 4819-4832.

[15] M. Kawasaki, Z. Horita and T. G. Langdon: Mater. Sci. Eng. A **524** (2009) 143-150.

[16] A. A. Salem, T. C. Langdon, T. R. Mcnelley, S. R. Kalidindi and S. L. Semiatin: Metall. Mater. Trans. A **37** (2006) 2879-2891.

[17] M.K. Wong, W. P. Kao, J. T. Lui, C. P. Chang and P.W. Kao: Acta Mater. **55** (2007) 715-725.

[18] J. May, D. Amberger, M. Dinkel, H. W. Höppel and M. Göken: Mater. Sci. Eng. A **483-484** (2008) 481-484.

[19] P. Charsley and L. J. Harris: Scr. Metall. **21** (1987) 341-344.

[20] P. Charsley, U. Bangert and L. J. Appleby: Mater. Sci. Eng. A **113** (1989) 231-236.

[21] M. Videm and N. Ryum: Mater. Sci. Eng. A **219** (1996) 1-10.

[22] T. Fujii, S. Uju, H. Tanaka, T. Murayama, C. Watanabe, S. Onaka and M. Kato: Plasticity, Failure and Fatigue in Structural Materials from Macro to Nano: Proc. the Hael Mughrabi Honorary Symposium, Ed. by K. J. Hsia, M.Göken, T. Pollock, P. D. Portella and N. R. Moody, (The Minerals, Metal & Materials Society, 2008) 123-127.

[23] Y. Nakanishi, H. Tanaka, T. Fujii, S. Onaka and M. Kato: Philos. Mag., submitted.

[24] P. Li, S. X. Li, Z. G. Wang and Z.F. Zhang: Acta Mater. **58** (2010) 3281-3294.

[25] Z. S. Basinski, A. S. Korbel and S. J. Basinski: Acta Metall. **28** (1980) 191-207.

[26] L. M. Brown: Mater. Sci. Eng. A **285** (2000) 35-42.

[27] L. M. Brown: Philos. Mag. **86** (2006) 4055-4068.

[28] H. Mughrabi and F. Pschenitzka: Philos. Mag. **85** (2005) 3029-3045.

[29] P. J. Wood: Philos. Mag. **28** (1973) 155-191.

[30] C. Laird: Mater. Sci. Eng. **81** (1986) 433-450.

[31] P. Lukáš and L. Kunz: Philos. Mag. **84** (2004) 317-330.

[32] O. B. Pedersen: Acta Metall. **38** (1990) 1221-1239.

[33] L. M. Brown: Metall. Trans. A **22** (1991) 1693-1708.

[34] O. B. Pedersen: Philos. Mag. **73** (1996) 829-858.

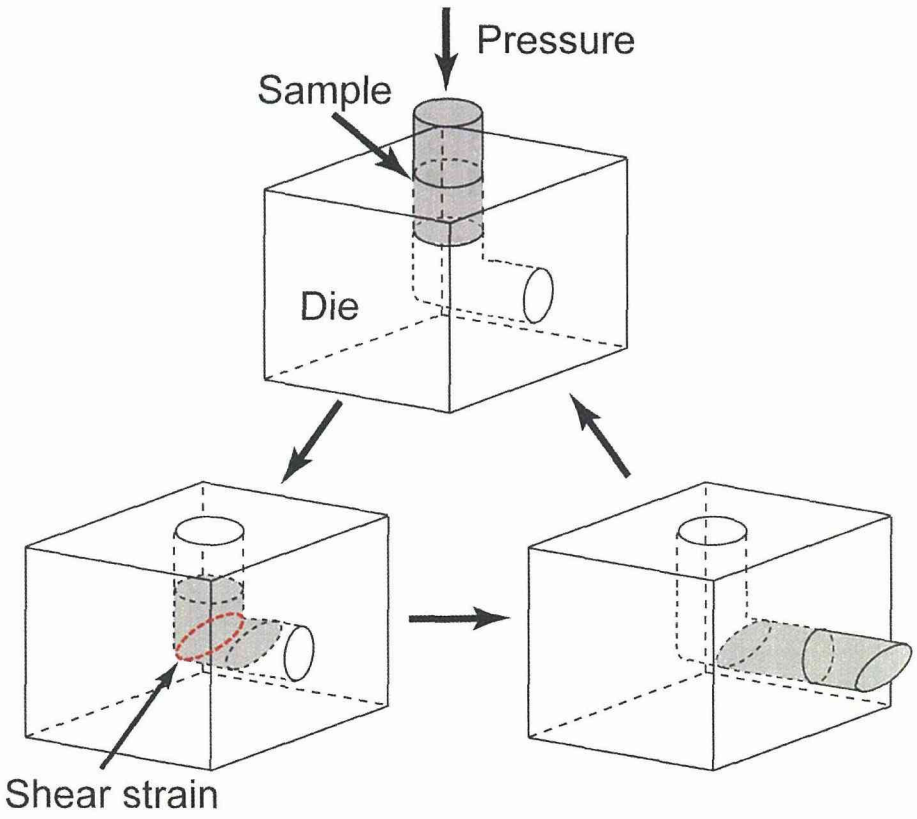

Figure 4-1. Schematic illustration showing the principle of the ECAP process.

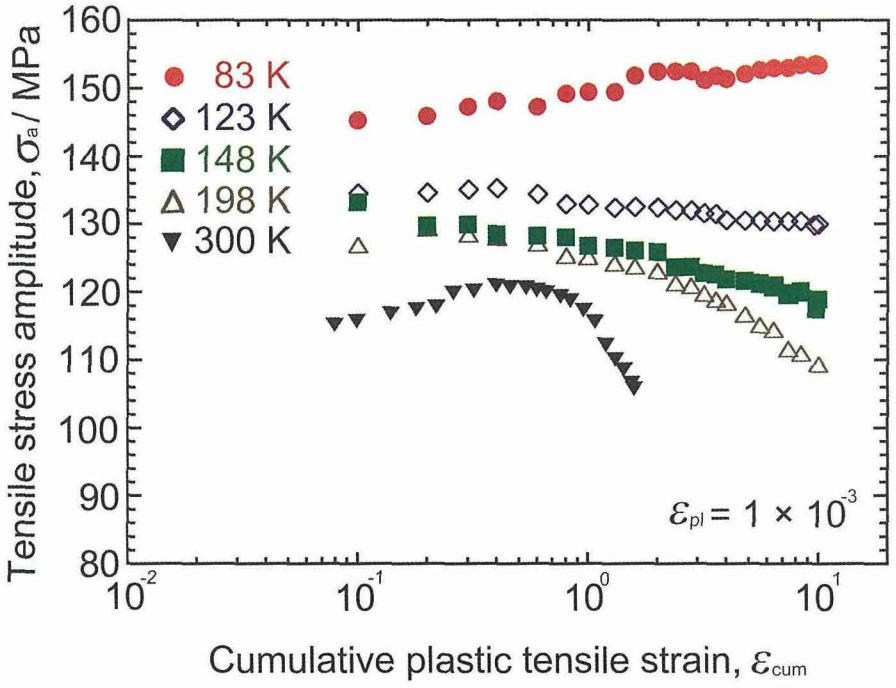

Figure 4-2. Cyclic hardening/softening curves of UFG Al fatigued under constant plastic tensile strain amplitude $\varepsilon_{pl} = 1\times10^{-3}$ at various temperatures.

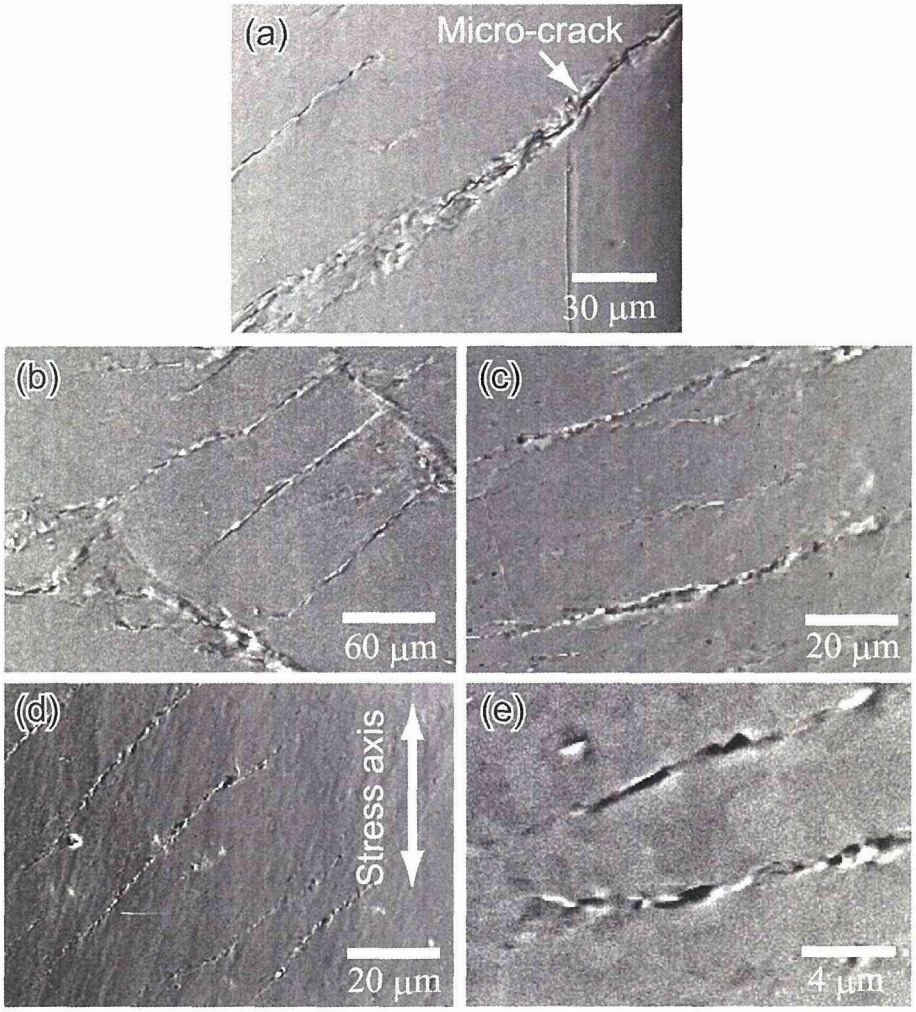

Figure 4-3. SEM images of micro-cracks and shear bands on the surface of specimens fatigued at (a) 300 K (The arrow shows a micro-crack), (b) 300 K, (c) 198 K, (d) 148 K and (e) 123 K. Note the different magnification for these photographs.

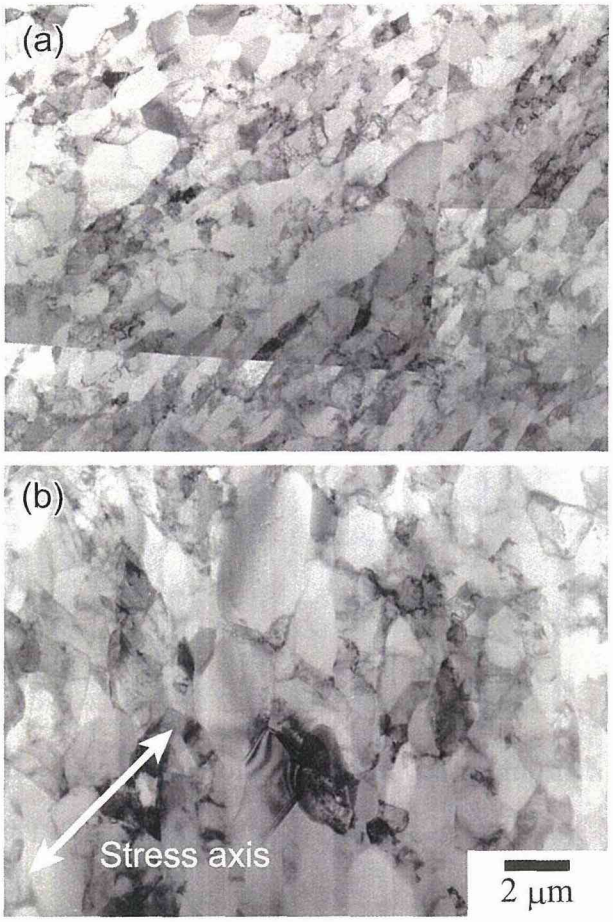

Figure 4-4. TEM photographs of UFG Al: (a) as-ECAPed specimen, (b) fatigued at 300 K. Stress axis inclines 45° to the vertical direction.

Figure 4-5. Occurrence of local grain coarsening in a specimen fatigued at 198 K.

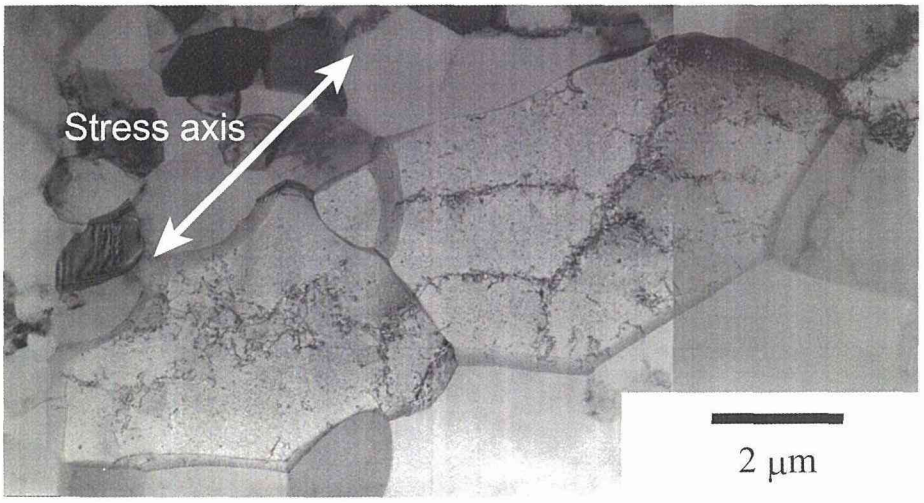

Figure 4-6. Dislocation cell formed in coarsened grains of a specimen fatigued at 198 K.

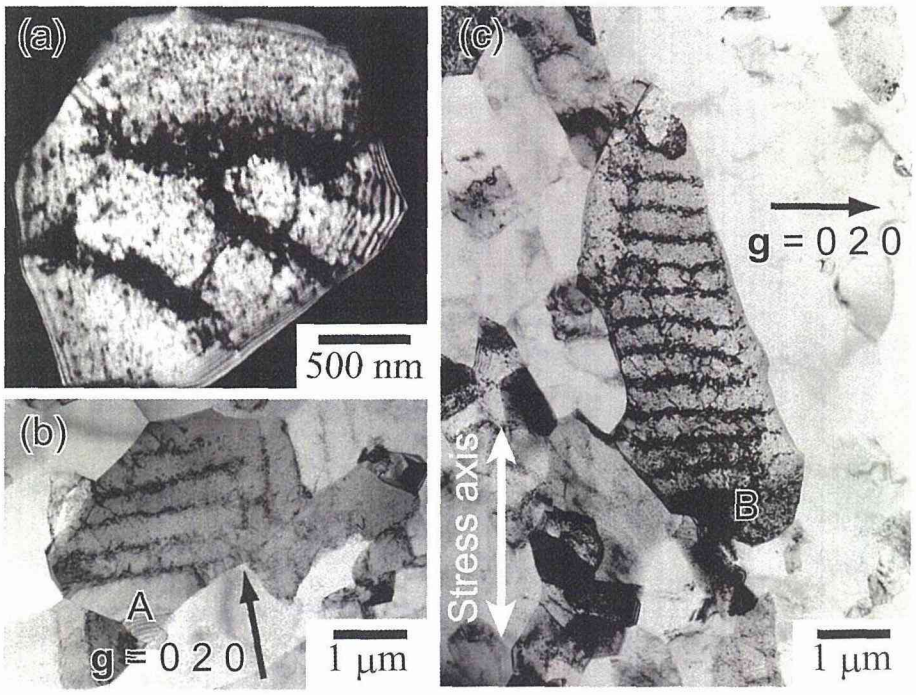

Figure 4-7. Dislocation cell (a) and wall ((b) and (c)) structures formed in fine grains of a specimen fatigued at 83 K. Zone axis of grain A and B: [001].

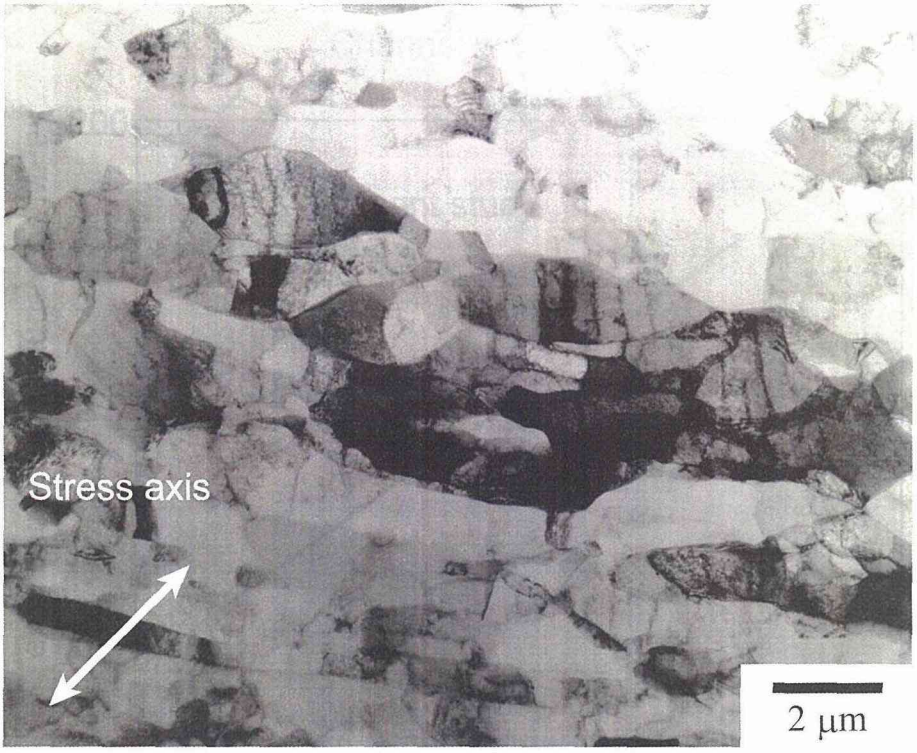

Figure 4-8. TEM photograph of UFG Al fatigued at 83 K. The fraction of grains that contain dislocation wall structure is about 50 %.

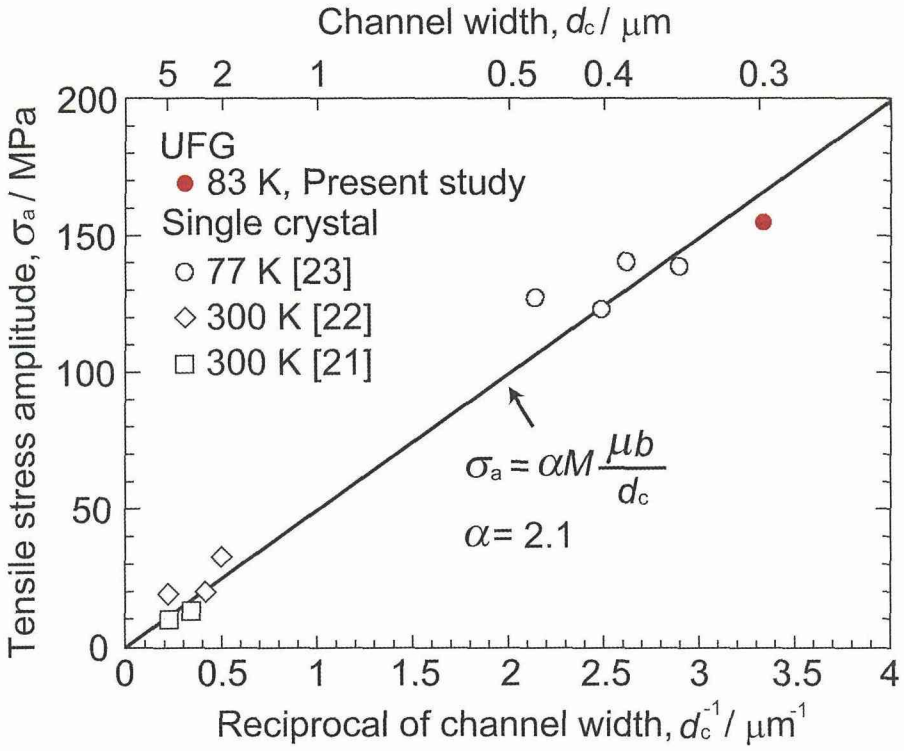

Figure 4-9. Relationship between tensile stress amplitude σ_a and reciprocal of channel width $1/d_c$. Experimental data for single-crystalline Al [21-23] and UFG Al are shown.

Chapter 5

Stability of fatigued dislocation wall structure in coarse-grained and ultrafine-grained aluminum against monotonic tensile deformation

5.1 Introduction

Ultrafine-grained (UFG) metals have been produced by severe plastic deformation (SPD) such as equal channel angular pressing (ECAP) [1], accumulative roll-bonding (ARB) [2] and high-pressure torsion (HPT) [3]. UFG fcc metals are known to show some characteristic physical and mechanical properties that are different from those of coarse-grained (CG) fcc metals, such as easier recrystallization and recovery [4-6], higher temperature and strain-rate dependencies of strength [7, 8] and deviation from the Hall-Petch relationship [9, 10]. In order to reveal the mechanism of such characteristic properties, many researchers have proposed various deformation models of UFG materials [11-27].

Cyclic deformation behavior of UFG metals is also unique and different from that of single-crystalline and CG metals. For high-cycle stress-controlled tests where strength is a major factor in determining the fatigue life, UFG metals show superior fatigue life compared with single-crystalline and CG metals [28-31]. On the other hand, UFG metals show deteriorated fatigue life for low-cycle strain-controlled fatigue tests where fatigue life is mainly controlled by ductility [28-31]. For the low-cycle tests, it is also known that UFG pure aluminum shows hardening followed by softening [28, 29] and distinct fatigue dislocation structure has not been observed in grains at room temperature [28]. In contrast, single-crystalline and CG Al show initial hardening, softening and secondary hardening [32-34] with the formation of characteristic dislocation structure such as vein [35, 36], wall [35, 36], labyrinth [32, 35, 37] and cell [28, 34] structures.

Although the cyclic deformation behavior of UFG Al is worth investigating more in detail, most reports were on commercially pure Al or on Al alloys. From the results of Chapter 4 and from our recent studies [38, 39], test temperature is known to play an important role on the cyclic deformation behavior of high purity UFG Al and very fine dislocation wall structure is formed when tested at 83 K in grains smaller than a few micrometers.

In this study, low-cycle fatigue tests were carried out under plastic-strain control at 77 K using CG and UFG Al, and monotonic tensile tests were performed in succession either at 300 K or 77 K after the fatigue tests. From the results of monotonic tensile tests and transmission electron microscopy (TEM), the formation and stability of the fatigued dislocation structure are studied.

5.2 Experimental procedure

High-purity Al (99.98 mass %) was used for the present study. Al sheets were annealed at 673 K for 2 h to obtain a fully recrystallized material. Average grain size of as-annealed Al was about 300 μm and this material will be referred to as as-annealed CG Al.

CG Al samples cut into a rod shape of 10 mm in diameter and 60 mm in length were prepared for the ECAP deformation at 300 K. Each rod was subjected to 8 passes of ECAP under route B_C (rotation by 90° in each pass) [1]. The ECAP was conducted at room temperature with a pressing speed of 16 mm s^{-1} and each rod is coated in a MoS_2 lubricant. After the ECAP deformation, average grain size of UFG Al became about 1.3 μm and this material will be referred to as as-ECAPed UFG Al.

The fatigue specimens with the gauge length of 10 mm and cross-sectional area of 5×6 mm^2 were taken from the central part of the as-ECAPed rods by spark erosion in the direction parallel to the rod axis. The specimens were mechanically polished with silicon-carbide paper and electrolytically polished using solution of 20 % perchloric acid and 80 % methanol.

Fully reversed tension-compression low-cycle fatigue tests were carried out at 77 K for these CG (as-annealed) and UFG (as-ECAPed) Al specimens under a constant plastic tensile strain amplitude of either $\varepsilon_{pl} = 1\times10^{-3}$ or 5×10^{-3} using an electro-hydraulic testing machine (Shimadzu Servopet). The specimens were immersed in liquid nitrogen to achieve the low temperature atmosphere during the fatigue tests. Strain was measured with an extensometer mounted directly on the gauge section and constant strain rate of 4×10^{-3} s^{-1} was employed using a triangular command signal. After reaching the saturation of tensile stress amplitude, fatigue tests were stopped at the cumulative plastic tensile strain ε_{cum} of 10 (for UFG Al) and 50 (for CG Al). Here, the cumulative plastic tensile strain is defined as

$$\varepsilon_{cum} = 4N\varepsilon_{pl} \tag{5-1}$$

where N is the number of fatigue cycles. Since UFG Al generally shows shorter fatigue life than CG Al at low-cycle fatigue tests [28, 29, 31], it is reasonable that UFG Al reached stress saturation at smaller cumulative plastic strain than CG Al. No cracks were observed on the surface of specimens after the fatigue tests mentioned above.

The tensile specimens with a gauge length of 10 mm and cross-sectional area of 1×3 mm^2 were sliced from the fatigue specimens and polished under the same conditions as those used to prepare fatigue specimens. Monotonic tensile tests were carried out at 300 K and 77 K for un-fatigued (as-annealed and as-ECAPed) and fatigued specimens at a constant strain rate of 4×10^{-3} s^{-1} using an Instron-type testing machine (Minebea TG-50kN).

The fatigued and monotonically deformed specimens were sliced into 3 mm diameter disks and ground down to a thickness of 0.2 mm with silicon-carbide paper. Then, the samples were electrolytically polished on a twin-jet polisher (Struers Tenupol-5) in solution of 8 % perchloric acid, 10 % 2-butoxyethanol and 82 % methanol. TEM observations were performed by using a JEOL 2011 microscope with an acceleration voltage of 200 kV.

As shown in Chapter 3 and 4, in order to the possibility of natural annealing and to ensure the preservation of dislocation structure until TEM observation, fatigued and deformed specimens were always stored in liquid nitrogen.

More concretely, specimens were handled very carefully so that they were exposed at

room temperature for less than 1 h between the fatigue and tensile tests and between the tensile tests and the TEM observation.

5.3 Results

5.3.1 Cyclic deformation behavior of CG and UFG Al

Figure 5-1 shows cyclic hardening curves of CG (as-annealed) and UFG (as-ECAPed) Al fatigued at 77 K. CG Al shows rapid hardening to saturation. At this test temperature, CG Al does not show either softening or secondary hardening characteristic of the room-temperature cyclic deformation behavior of single-crystalline and CG Al [31-33]. The saturation stress of CG Al in this study was 118 MPa ($\varepsilon_{pl} = 1\times10^{-3}$) and 126 MPa ($\varepsilon_{pl} = 5\times10^{-3}$).

The cyclic deformation behavior of UFG Al at 77 K is similar to that of CG Al at 77 K. UFG Al shows slight hardening followed by stress saturation. The saturation stress of UFG Al in this study was 151 MPa ($\varepsilon_{pl} = 1\times10^{-3}$) and 186 MPa ($\varepsilon_{pl} = 5\times10^{-3}$). Since UFG Al has experienced extensive work hardening during the ECAP deformation, it is natural that cyclic hardening rate of UFG Al is lower compare to that of CG Al.

5.3.2 Monotonic tensile deformation behavior of fatigued Al

The tensile stress-strain curves at 300 K and 77 K of as-annealed and fatigued CG Al are shown in Fig. 5-2. For both as-annealed and fatigued CG Al, the ultimate tensile strength (UTS) and tensile ductility are larger at 77 K than at 300 K. When test temperature is the same, fatigued CG Al shows much higher yield strength and much lower tensile ductility than as-annealed CG Al.

The monotonic tensile deformation behavior of UFG Al was quite different from that of CG Al. Figure 5-3 shows the tensile stress-strain curves of as-ECAPed and fatigued UFG Al monotonically deformed at 300 K and 77 K. There are at least two remarkable points to

be noted in Fig. 5-3. First, regardless of as-ECAPed or fatigued UFG Al, UTS and tensile ductility at 77 K are much higher than those at 300 K. Secondly, UFG Al at 77 K maintains high UTS and high tensile ductility even after the fatigue tests. These findings will be discussed later.

5.3.3 Microstructural observation

TEM images taken from fatigued and deformed specimens of CG Al are shown in Fig. 5-4 (a) to (c). After the fatigue tests of CG Al, fine dislocation walls were found to be developed in all grains (Fig. 5-4 (a)). These dislocation walls were nearly parallel to the (010) plane. It appears that two mutually perpendicular sets of walls exist in Fig. 5-4 (c). These walls are considered to form layers, just like the labyrinth walls [32, 35, 37]. The average channel width between adjacent walls was about 350 nm ($\varepsilon_{pl} = 1\times10^{-3}$) and about 330 nm ($\varepsilon_{pl} = 5\times10^{-3}$). The absence of contrast variation among the channels indicates that the walls are made of edge dislocation dipoles. As will be discussed later, the observed channel widths in this study are much narrower than the frequently observed widths between 1 to 4 μm in single-crystalline and CG Al fatigued at room-temperature [32, 37].

What should also be noted in Fig. 5-4 is that dislocation walls formed during cyclic deformation in CG Al persists even after monotonic tensile tests at 300 K and 77 K and no distinct change in the dislocation wall structure was noted before and after the monotonic tensile tests (Fig. 5-4 (b) and (c)).

Figures 5-5 (a) to (d) show TEM images taken from fatigued and deformed specimens of UFG Al. Similar to CG Al, dislocation walls nearly parallel to (010) are found to be formed in many grains of UFG Al and the average channel width was about 320 nm ($\varepsilon_{pl} = 1\times10^{-3}$) and about 300 nm ($\varepsilon_{pl} = 5\times10^{-3}$). From the observation such as that in Fig. 5 (b), it was found that the fraction of grains that contain dislocation wall structure is nearly 50 %. Considering the TEM visibility condition of dislocations, actual fraction may be larger. As is well known, dislocation multiplication and rearrangement are necessary to form certain fatigue dislocation structure including the present wall structure. If grain size is

smaller, such dislocation activities would become more difficult due to smaller space and stronger constraint by the surrounding grain boundaries. Therefore, it is natural that the larger the grain size, the easier the formation of dislocation wall structure.

It is very interesting to find from Fig. 5-5 that dislocation wall structure formed during fatigue tests at 77 K disappears after succeeding monotonic tensile deformation (Fig. 5-5 (c) and (d)). As described earlier, dislocation wall structure in CG Al persists even after monotonic tensile deformation at both test temperatures (Fig. 5-4 (a) to (c)). Therefore, this disappearance of the wall structure is characteristic of UFG Al suggesting that the dislocation wall structure formed during fatigue tests in UFG Al is unstable against succeeding monotonic tensile deformation.

5.4 Discussion

5.4.1 Dependence of the channel width on stress amplitude

The average channel width of CG and UFG Al fatigued at 77 K are much smaller than that of single-crystalline and CG Al fatigued at 300 K [32, 37]. As shown in Chapters 3 and 4, there is a linear relationship between tensile stress amplitude σ_a and the reciprocal of channel width $1 / d_c$ [40], *i. e.*,

$$\tau_a = \frac{\alpha M \mu b}{d_c} \tag{5-2}$$

where α is a dimensionless constant to be determined, M the Taylor factor of 3.06, μ the shear modulus and b the magnitude of the Burgers vector. With μ = 26.7 GPa and b = 0.286 nm, calculated values of the constant α are shown in Table 1. According to theoretical studies by Brown [41, 42] and Pedersen [43, 44], the value of α is estimated to be 2.0. Therefore, the calculated values of α listed in Table 1 are close to the theoretical value.

Figure 5-6 summarizes the experimental results of the reciprocal of channel width under a given stress amplitude for single-crystalline Al [32, 37, 45], UFG Al [39], CG Al and

UFG Al in this study. From the slope of the straight line, it was found that $\alpha = 2.0$ which is again in good agreement with the theoretically-estimated value.

5.4.2 Relationship between monotonic tensile deformation behavior and microstructural stability of CG and UFG Al

The enhanced ductility of both CG and UFG Al at 77 K compared with that at 300 K (Figs. 5-2 and 5-3) has been known for many years. Some investigators have reported that both UTS and ductility of UFG Al become larger with decreasing temperature [9, 46, 47]. The larger UTS is a natural result of strong temperature dependence of strength in UFG materials [25-27, 48]. On the other hand, the larger ductility is mainly due to larger work hardening at 77 K than at 300 K. Since larger work hardening increases the stability of plastic deformation and, thus, delays the formation of necking in tensile specimens, it can be understood that both strength and ductility increases at 77 K than at 300 K regardless of the grain size.

In this study, it was demonstrated that the effect of fatigue tests on succeeding monotonic tensile deformation behavior is quite different between CG and UFG Al. Let us first discuss the experimental results for CG Al. The fact that fatigued CG Al showed much higher yield strength and lower ductility than as-annealed CG Al (Fig. 5-2) can be understood reasonably since CG Al has experienced large cyclic hardening during the fatigue tests (Fig. 5-1). Dislocation wall structure is formed in all CG grains and it persists after monotonic tensile deformation (Fig. 5-4 (b) and (c)). The persisting walls act as strong barriers against tensile deformation. Therefore, it is natural that fatigued CG Al shows much higher yield strength and lower tensile ductility than as-annealed CG Al.

The characteristic finding for the UFG Al is, on the other hand, that dislocation wall structure formed in UFG Al disappears completely during monotonic tensile deformation at both 300 K and 77 K (Fig. 5-5 (c) and (d)). As mentioned previously, since all the specimens were store in liquid nitrogen in this study, the disappearance of the dislocation wall structure after monotonic tensile deformation is not due to the natural recovery. That is,

monotonic tensile tests certainly accelerate the disappearance of dislocation wall structure.

It is notable that fatigued UFG Al shows nearly the same UTS and tensile ductility as as-ECAPed Al at both temperatures. Therefore, the observed high UTS and ductility in as-ECAPed and fatigued UFG Al are believed to have something to do with the disappearance of the dislocation structure. Figure 5-7 (a) and (b) show the microstructure of UFG Al fatigued at 77 K with $\varepsilon_{pl} = 1\times10^{-3}$ and monotonically deformed at 77 K till a strain of 0.007 and 0.15, respectively. In Fig 5-7 (a), broken traces of dislocation wall structure can be seen. However, at the strain of 0.15 (Fig. 5-7 (b)), neither dislocation wall structure nor its traces can be seen any more. These results indicate that dislocation wall structure in UFG Al disappears in the early stages of succeeding monotonic tensile deformation and acts at most as weak barriers against dislocation motion during monotonic tensile deformation.

Why is the dislocation structure formed in UFG Al less stable than that in CG Al? It is known that store energy introduced in materials increases with increasing the number of ECAP passes [5, 49]. For ECAPed Cu [4, 5] and HPTed Ni [6], recovery and recrystallization are known to take place more easily at lower temperatures than conventional recrystallization temperature of near 0.5 T_m (T_m: melting temperature). Recrystallization temperature decreases with increasing the stored energy [5]. Moreover, Molodova *et al.* [4] reported that the apparent activation energy Q_R for recrystallization of ECAPed Cu decreases significantly with increasing the number of ECAP passes; Q_R decreases from 1 eV at 1 pass to 0.7 eV at 8 passes. These reports indicate that higher stored energy causes UFG materials energetically unstable and results in the larger driving force for recovery and recrystallization. Such low thermal stability of UFG materials [4-6, 49] would explain, at least qualitatively, the easy disappearance of the dislocation wall structure.

Formation of dislocation wall structure is often related to the formation of persistent slip bands, surface intrusions and extrusions that are detrimental to fatigue resistance [50, 51]. However, since grain size is very small and since the unstable dislocation wall structure is formed only in selected grains of UFG Al, the dislocation walls do not appear to cause the extensive formation of persistent slip bands. From this viewpoint, the present unstable

dislocation walls formed in UFG Al at 77 K may not be so harmful to the fatigue resistance. This is most probably the reason why ECAPed and fatigued UFG Al maintains nearly the same tensile strength and ductility as as-ECAPed UFG Al. Further studies are needed to discuss in more detail the relationship between the fatigue resistance and the degree of microstructural stability of UFG materials.

5.5 Conclusions

The low-cycle fatigue tests of high purity CG and UFG Al (99. 98 mass %) were carried out at 77 K. After the fatigue tests, CG and UFG Al were deformed in tension at 300 K and 77 K. The results and findings are summarized as follows.

(1) During the strain-controlled fatigue tests, both CG and UFG Al show hardening to stress saturation at 77 K. The cyclic hardening rate of UFG Al is lower compare to that of CG Al.

(2) Fatigued CG Al shows much higher yield strength and lower tensile ductility than as-annealed CG Al at 300 K and 77 K. On the other hand, fatigued UFG Al shows almost the same yield strength and ductility as as-ECAPed UFG Al at both 300 K and 77K.

(3) Fine dislocation wall structure is formed in all the CG grains during fatigue at 77 K. This dislocation wall structure in CG Al persists after monotonic tensile deformation at both 300 K and 77 K.

(4) Very fine dislocation wall structure is formed in UFG Al during fatigue tests at 77 K and the fraction of the grains that contain the dislocation wall structure is about 50 %. The dislocation wall structure in UFG Al is found to disappear easily during the early stages of monotonic tensile deformation.

(5) Good correlation is found between the reciprocal of the channel width and the saturation stress amplitude, from single-crystalline Al to UFG Al.

(6) Relatively unstable dislocation wall structure in UFG Al acts as a weak barrier for dislocation motion in monotonic tensile tests and may not be harmful in reducing the fatigue resistance.

References

[1] Y. Iwahashi, Z. Horita, M. Nemoto and T. G. Langdon: Acta Mater. **46** (1998) 3317-3331.

[2] Y. Saito, N. Tsuji, H. Utsunomiya and S. Tanigawa: Scr. Mater. **39** (1998) 1221-1227.

[3] Z. Horita and T. G. Langdon: Mater. Sci. Eng. A **410-411** (2005) 422-425.

[4] X. Molodova, G. Gottstein, M. Winning and R. J. Hellmig: Mater. Sci. Eng. A **460-461** (2007) 204-213.

[5] Y. Zhang, J. T. Wang, C. Cheng and J. Liu: J. Mater. Sci. **43** (2008) 7326-7330.

[6] H. W. Zhang, X. Huang, R. Pippan and N. Hansen: Acta Mater. **58** (2010) 1698-1707.

[7] Q. Wei, S. Cheng, K. T. Ramesh and E. Ma: Mater. Sci. Eng. A **381** (2004) 71-79.

[8] T. Kunimine, N. Takata, N. Tsuji, T. Fujii, M. Kato and S. Onaka: Mater. Trans. **50** (2009) 64-69.

[9] C. Y. Yu, P. W. Kao and C. P. Chang: Acta Mater. **53** (2005) 4019-4028.

[10] N. Kamikawa, X. Huang, N. Tsuji and N. Hansen: Acta Mater. **57** (2009) 4198-4208.

[11] R. O. Scattergood and C. C. Koch: Scr. Metall. Mater. **27** (1992) 1195-1200.

[12] J. Lian, B. Baudelet and A. A. Nazarov: Mater. Sci. Eng. A**172** (1993) 23-29.

[13] R. A. Masumura, P. M. Hazzledine and C. S. Pande: Acta Mater. **46** (1998) 4527-4534.

[14] D. Jia, Y. M. Wang, K. T. Ramesh, E. Ma, Y. T. Zhu and R. Z. Valiev: Appl. Phys. Lett. **79** (2001) 611-613.

[15] H. Van Swygenhoven, H. Caro and D. Farkas: Mater. Sci. Eng. A **310-311** (2001) 440-444.

[16] E. Nes and K. Mathinsen: Mater. Sci. Eng. A **322** (2002) 176-193.

[17] Y. M. Wang, E. Ma and M. W. Chen: Appl. Phys. Lett. **80** (2002) 2395-2397.

[18] S. Chen, J. A. Spencer and W. W. Milligan: Acta Mater. **51** (2003) 4505-4518.

[19] A. Hasnaoui, P. M. Derlet and H. Van Swygenhoven: Acta Mater. **52** (2004) 2251-2258.

[20] H. S. Kim and Y. Estrin: Acta Mater. **53** (2005) 765-772.

[21] R. J. Asaro and S. Suresh: Acta Mater. **53** (2005) 3369-3382.

[22] G. Saada: Philos. Mag. **85** (2005) 3003-3018.

[23] M. A. Meyers, A. Mishra and D. J. Benson: Prog. Mater. Sci. **51** (2006) 427-556.

[24] R. W. Armstrong and P. Rodriguez: Philos. Mag. **86** (2006) 5787-5796.

[25] Y. M. Wang, A. V. Hamza and E. Ma: Acta Mater. **54** (2006) 2715-2726.

[26] M. Kato, T. Fujii, S. Onaka: Mater. Trans. **49** (2008) 1278-1283.

[27] M. Kato: Mater. Sci. Eng. A **516** (2009) 276-282.

[28] M.K. Wong, W. P. Kao, J. T. Lui, C. P. Chang and P.W. Kao: Acta Mater. **55** (2007) 715-725.

[29] J. May, D. Amberger, M. Dinkel, H. W. Höppel and M. Göken: Mater. Sci. Eng. A **483-484** (2008) 481-484.

[30] S. Malekjani, P. D. Hodgson, P. Cizek, I. Sabirov and T. B. Hilditch: Int. J. Fatigue **33** (2011) 700-709.

[31] M. Soliman, E. A. El-Danaf and A. A. Almajid: Mater. Sci. Eng. A **532** (2012) 120-129.

[32] M. Videm and N. Ryum: Mater. Sci. Eng. A **219** (1996) 1-10.

[33] M. Videm and N. Ryum: Mater. Sci. Eng. A **219** (1996) 11-20.

[34] T. Fujii, N. Sawatari, S. Susumu and M. Kato: Mater. Sci. Eng. A **387-389** (2004) 486-490.

[35] P. Charsley and L. J. Harris: Scr. metall. **21** (1987) 341-344.

[36] P. Charsley, U. Bangert and L. J. Appleby: Mater. Sci. Eng. A **113** (1989) 231-236.

[37] T. Fujii, S. Uju, H. Tanaka, T. Murayama, C. Watanabe, S. Onaka and M. Kato: Plasticity, Failure and Fatigue in Structural Materials from Macro to Nano: Proceedings of the Hael Mughrabi Honorary Symposium, Ed. by K. J. Hsia, M.Göken, T. Pollock, P. D. Portella and N. R. Moody, (The Minerals, Metals & Material Society, 2008) 123-127.

[38] Y. Nakanishi, T. Fujii, S. Onaka and M. Kato: Proc. 12th Int. Conf. on Aluminium Alloys, ed. by S. Kumai, O. Umezawa, Y. Takayama, T. Tsuchida and T. Sato, (The Japan Inst. Light Metals, 2010) 326-331.

[39] Y. Nakanishi, T. Fujii, S. Onaka and M. Kato: Mater. Trans. **52** (2011) 890-894.

[40] Z. S. Basinski, A. S. Korbel and S. J. Basinski: Acta Metall. **28** (1980) 191-207.

[41] L. M. Brown: Mater. Sci. Eng. A **285** (2000) 35-42.

[42] L. M. Brown: Metall. Trans. A **22** (1991) 1693-1708.

[43] O. B. Pedersen: Acta. Metall. **38** (1990) 1221-1239.

[44] O. B. Pedersen: Philos. Mag. **73** (1996) 829-858.

[45] Y. Nakanishi, H. Tanaka, T. Fujii, S. Onaka and M. Kato: Philos. Mag., submitted.

[46] P. L. Sun, E. K. Cerreta, J. F. Bingert, G. T. GrayIII and M. F. Hundley: Mater. Sci. Eng A **464** (2007) 343-350.

[47] Y. Z. Estrin: Low Temp. Phys. **34** (2008) 665-671.

[48] G. A. Malygin: Phys. Solid State **49** (2007) 961-982.

[49] W. Q. Cao, C. F. Gu, E. V. Pereloma and C.H. J. Davies: Mater. Sci. Eng. A **492** (2008) 74-79.

[50] P. Lukáš and L. Kunz: Philos. Mag. **84** (2004) 317-330.

[51] N. Thompson, N. J. Wadsworth and N. Louat: Philos. Mag. **1** (1956) 113-126.

Table 1. Experimental values of tensile stress amplitude σ_a and channel width d_c and calculated values of the constant α for CG Al and UFG Al.

	Tensile stress amplitude: σ_a [MPa]	Channel width: d_c [nm]	Dimensionless constant: α
CG: $\varepsilon_{pl} = 1 \times 10^{-3}$	118	350	1.7
CG: $\varepsilon_{pl} = 5 \times 10^{-3}$	126	330	1.8
UFG: $\varepsilon_{pl} = 1 \times 10^{-3}$	151	320	2.0
UFG: $\varepsilon_{pl} = 5 \times 10^{-3}$	186	300	2.4

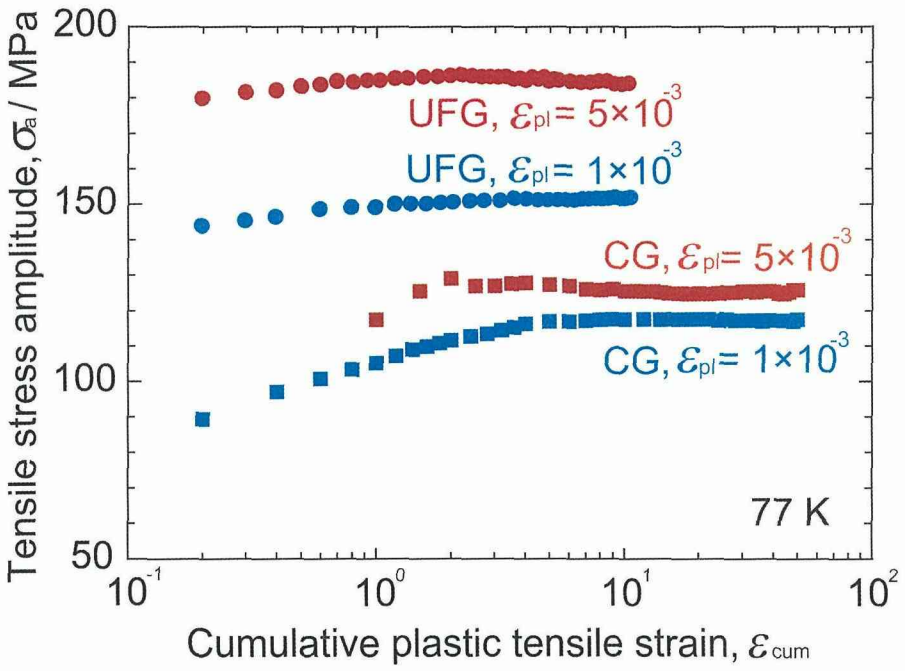

Figure 5-1. Cyclic hardening curves of CG and UFG Al fatigued under constant plastic tensile strain amplitudes $\varepsilon_{pl} = 1\times10^{-3}$ and 5×10^{-3} at 77 K.

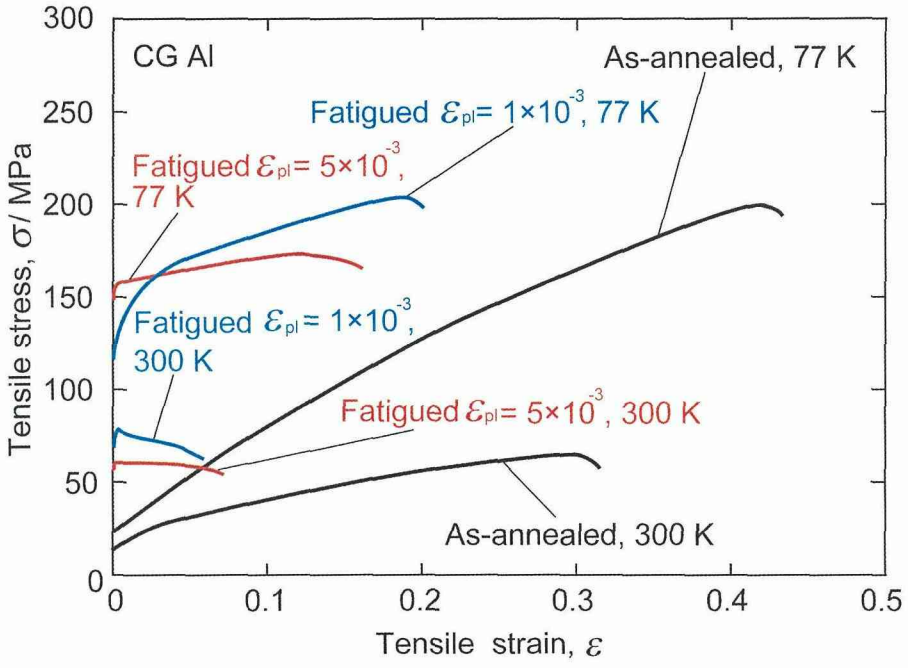

Figure 5-2. Tensile stress-strain curves at 300 K and 77 K of as-annealed and fatigued CG Al.

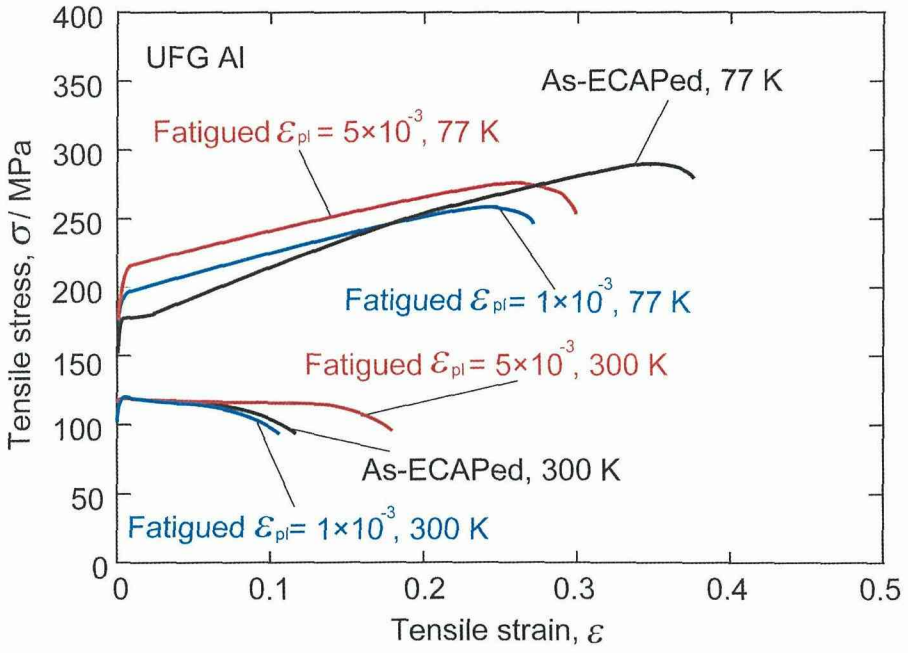

Figure 5-3. Tensile stress-strain curves at 300 K and 77 K of as-ECAPed and fatigued UFG Al.

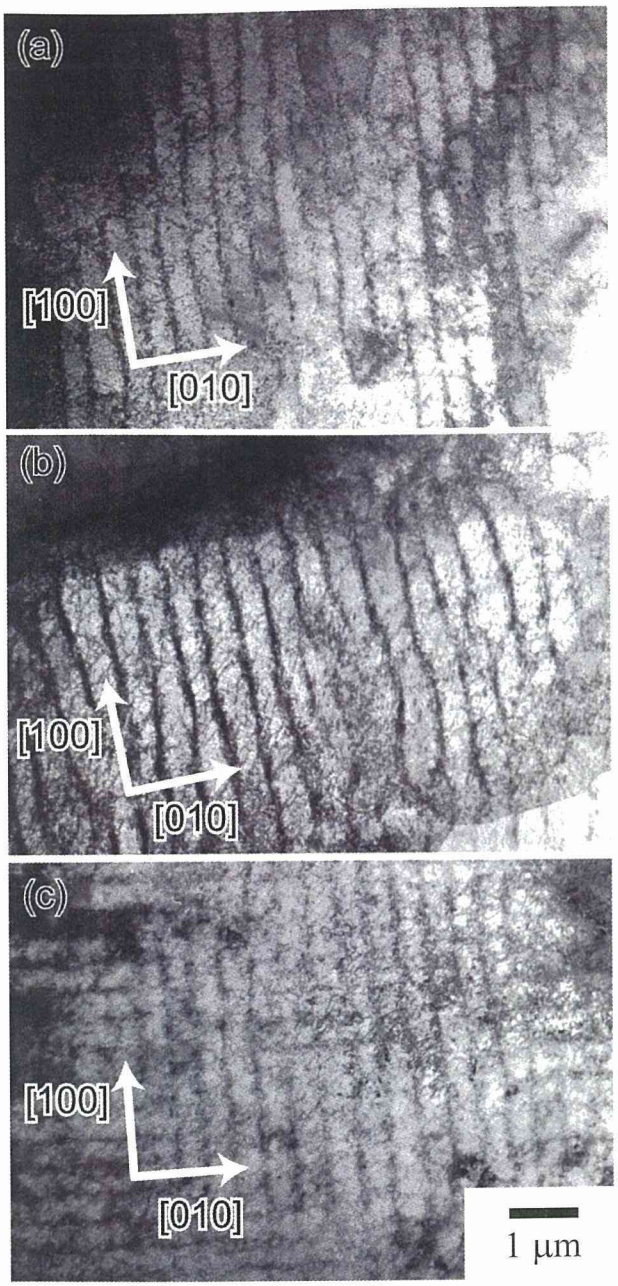

Figure 5-4. TEM photographs of CG Al: (a) fatigued at 77 K with $\varepsilon_{pl} = 5\times10^{-3}$, (b) fatigued at 77 K with $\varepsilon_{pl} = 5\times10^{-3}$ and then monotonically deformed till failure at 300 K, (c) fatigued at 77 K with $\varepsilon_{pl} = 5\times10^{-3}$ and then monotonically deformed till failure at 77 K. Zone axis: [001].

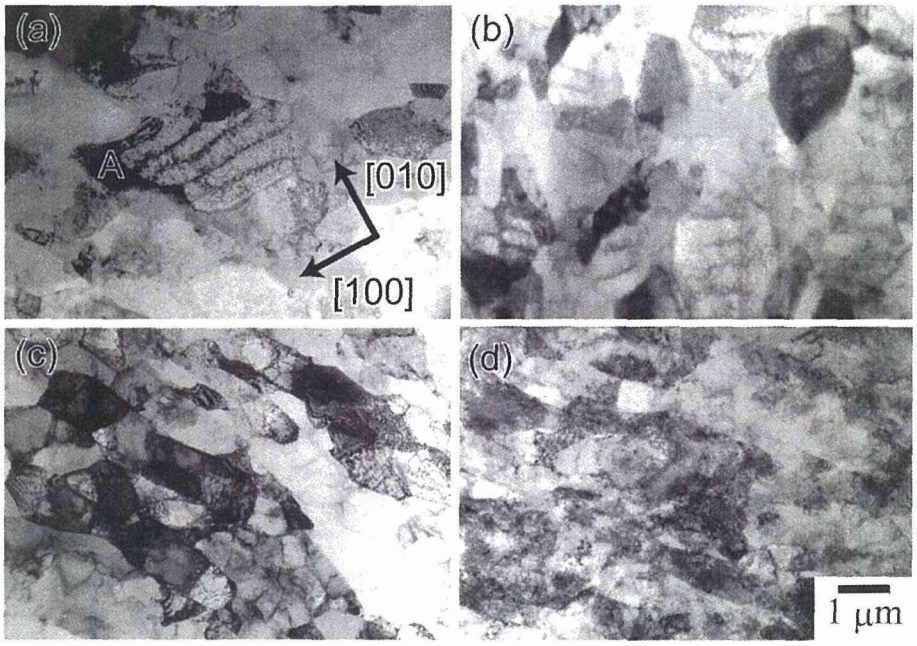

Figure 5-5. TEM photographs of UFG Al: (a) fatigued at 77 K with $\varepsilon_{pl} = 5\times10^{-3}$, zone axis of grain A: [001], (b) fatigued at 77 K with $\varepsilon_{pl} = 5\times10^{-3}$. The fraction of grains that contain dislocation wall structure is about 50 %, (c) fatigued at 77 K with $\varepsilon_{pl} = 5\times10^{-3}$ and then monotonically deformed till failure at 300 K, (d) fatigued at 77 K with $\varepsilon_{pl} = 5\times10^{-3}$ and then monotonically deformed till failure at 77 K.

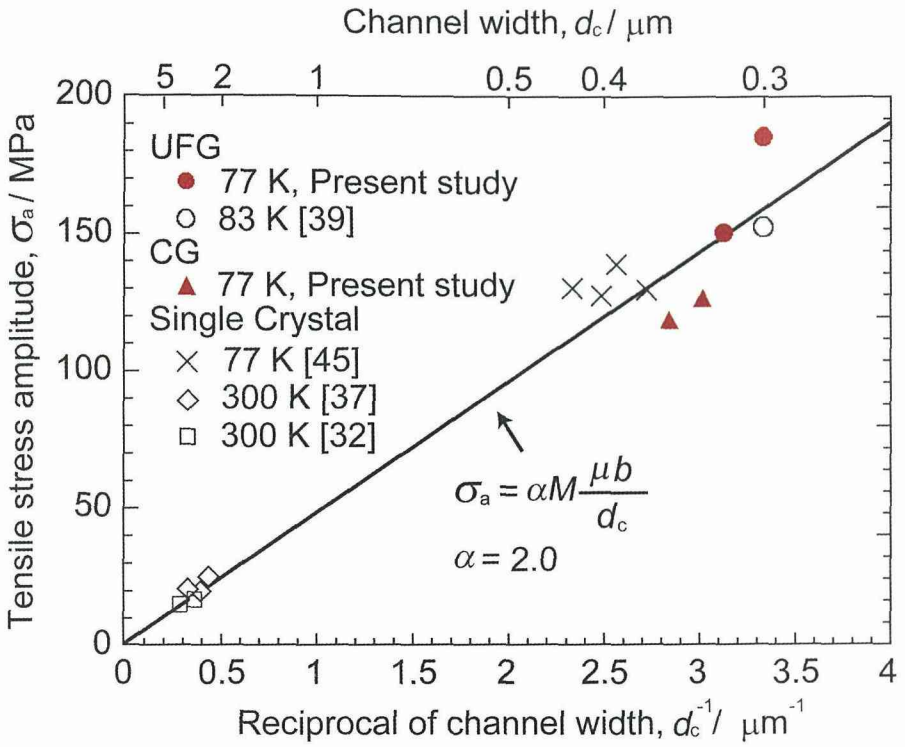

Figure 5-6. Relationship between tensile stress amplitude σ_a and the reciprocal of channel width $1/d_c$. Experimental data for single-crystalline Al, CG Al and UFG Al are shown. Reference numbers are shown in the brackets [32, 37, 39, 45].

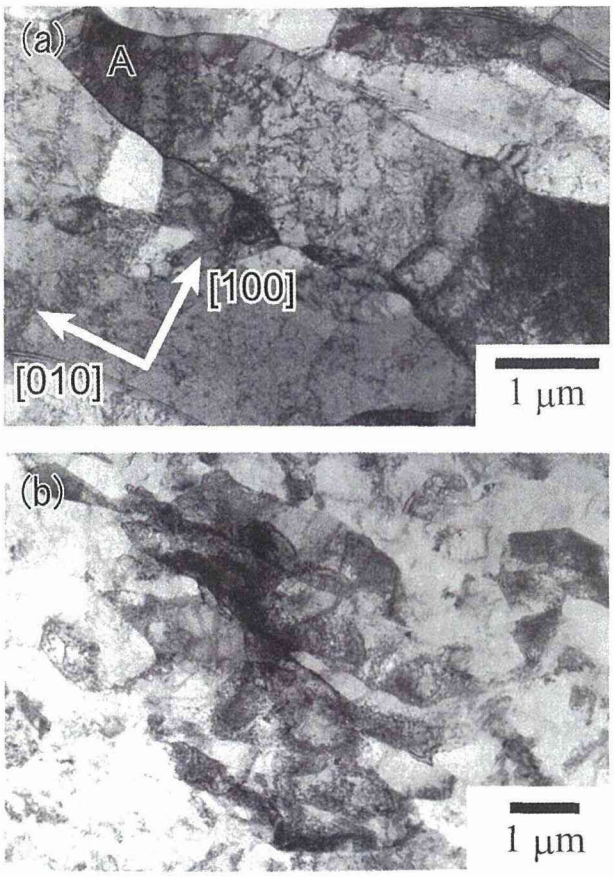

Figure 5-7. TEM photographs of UFG Al fatigued at 77 K with ε_{pl} =1×10^{-3} and then deformed in tension at 77 K, (a) monotonic tensile test stopped at ε = 0.007, zone axis of grain A: [001], (b) monotonic tensile test stopped at ε = 0.15.

Chapter 6
General conclusions

6.1 Summary and conclusions of the present dissertation

In this study, the effects of test temperature on cyclic deformation behavior and microstructural development in single-crystalline, coarse-grained (CG) and ultrafine-grained (UFG) Al have been described. Moreover, the stability of dislocation wall structure in CG and UFG Al against succeeding monotonic tensile deformation has been investigated.

In Chapter 1, "General Introduction", the background and overall objectives of the present dissertation were described.

In Chapter 2, "Cyclic deformation behavior and microstructure of fcc metals: survey and perspective", cyclic deformation behavior and microstructural development of single-crystalline, CG and UFG fcc metals were overviewed and the purpose and importance of this dissertation was shown.

In Chapter 3, "Low-temperature cyclic deformation of aluminum single crystals", cyclic deformation behavior and microstructural development of Al single crystals at 77 K have been investigated. At 77 K, Al single crystals showed saturation stress in cyclic hardening curves and stress plateau of 43 MPa in a range of plastic shear strain from 2×10^{-3} to 2×10^{-2} in the cyclic stress-strain curve. The persistent slip bands (PSBs) were formed parallel to the primary slip planes during cyclic deformation at 77 K and well-developed {100} walls were formed in the PSBs. Good correlation was found between the reciprocal of the channel width of the dislocation walls and the saturation stress. Therefore, it is concluded that PSBs carry the applied plastic strain and their volume fraction increases with increasing plastic strain amplitude. From surface observation and trace analysis, the {100}

walls in PSBs were found to be formed by the activation of multiple slip systems, *i.e.* the primary and critical slip systems and the microstructure in PSBs was characterized as labyrinth structure. From the experimental results, it has been found that both temperature and SFE play important roles in the cyclic deformation behavior and the microstructural development of pure Al single crystals: The existence of the stress plateau can be explained by the temperature effect and the occurrence of the multiple slip systems and the formation of two {100} dislocation walls can be explained by the SFE effect.

In Chapter 4, "Low-temperature cyclic deformation of UFG aluminum", temperature dependence of cyclic deformation behavior and microstructural development in UFG Al have been investigated. With decreasing the test temperature, the amount of cyclic softening became less significant, the fraction of shear band decreased, fraction of coarsened grain decreased and formation of dislocation cell and wall structures became easier. At 83 K, well developed dislocation walls were formed in fine grains. Good correlation was found between the reciprocal of the channel width of the dislocation walls and the saturation stress for single-crystalline and UFG Al. Therefore, the channel width of dislocation walls of UFG Al is also determined by the stress amplitude in the same manner as that of single-crystalline and CG Al.

In Chapter 5, "Stability of fatigued dislocation wall structure in CG and UFG aluminum against monotonic tensile deformation", monotonic tensile tests were carried out for CG and UFG Al at 300 K and 77 K soon after low-cycle strain-controlled fatigue tests at 77 K. When monotonic tensile tests were conducted at the same temperature, fatigued CG Al showed much higher yield strength and much lower tensile ductility than as-annealed CG Al. Regardless of whether UFG Al was subjected the fatigue tests or not, both ultimate tensile strength (UTS) and tensile ductility of UFG Al at 77 K were much higher than those at 300 K. Moreover, UFG Al at 77 K maintained high UTS and high tensile ductility even after the fatigue tests. Dislocation wall structure in CG Al persisted even after monotonic tensile tests at 300 K and 77 K. On the other hand, dislocation wall structure in UFG Al disappeared easily during the early stages of monotonic tensile deformation. From the

results of these monotonic tensile tests and microstructural observation, it is concluded that the relatively unstable dislocation wall structure in UFG Al act as a weak barrier for dislocation motion in monotonic tensile tests.

6.2 Future studies

In the present study, many new results as shown above were obtained on the temperature dependence of cyclic deformation behavior and microstructural development for single-crystalline, CG and UFG Al. Furthermore, the difference in the stability of dislocation wall structure against monotonic tensile deformation between CG and UFG Al has been found and investigated for the first time in the research history of cyclic deformation of Al. In the following, some problems to be examined will be listed to emphasize that many more research opportunities are waiting for us in this fascinating area of the cyclic deformation of fcc metals.

The effects of temperature and SFE on cyclic deformation behavior and microstructural development of Al have been studied in Chapter 3. However, the dependence of crystal orientation on the cyclic deformation and microstructural development of Al single crystals at 77 K has not been investigated. For Cu single crystals, on the other hand, the formation of dislocation structure, such as ladder, labyrinth and cell structures, is known to depend on strain amplitude and crystal orientation. For the comprehensive understanding of the fatigue mechanism of fcc metals, the cyclic deformation behavior of Al single crystals with various crystal orientations at 77 K is worth investigating.

As shown in Chapter 4, shear band formation, microstructural development and grain coarsening are the three important factors to characterize the low-temperature cyclic deformation behavior of UFG Al. Indeed, these three factors can be mutually related to each other. For example, one may think that dislocation structures are formed preferentially at shear band regions with concentrated plastic deformation. If this is the case, however, dislocation structures must have developed more easily at higher temperatures where shear

bands appear more frequently. Instead, the experimental results are the opposite, as shown in section 4.3.2 and 4.3.3. Therefore, the present study indicated that high enough stresses are necessary for fine cell and wall structures to be formed in small grains of fatigued UFG Al. However, the relationship between the shear-band formation and grain coarsening, for example, has not yet been revealed.

As described in Chapter 5, dislocation wall structure in UFG Al is less stable against monotonic tensile deformation than that in CG Al. In this study, the reason why dislocation wall structure in UFG Al disappears easily has been attributed rather qualitatively to the low thermal stability which comes from high stored energy of UFG materials. However, the relationship between the stability of dislocation structure in UFG Al and low thermal stability of UFG materials has not been understood quantitatively. Therefore, the remaining research subject will be the quantitative understanding of the stability of dislocation structure in UFG metals against monotonic tensile deformation: for example, investigation of the stability of dislocation structure by using ECAP Al subjected to various ECAP passes (various stored energies) would be very interesting.

In concluding this dissertation, I sincerely hope that the results and findings shown in this study will greatly contribute to the comprehensive understanding of the fatigue mechanisms of single-crystalline, CG and UFG fcc metals.

Acknowledgements

This work was conducted with the encouragements and support of Professor Masaharu Kato, my advisor. His enthusiastic discussions and insightful advices provided a strong motivation during the course of study. I have been impressed by not only his deep and wide knowledge but also his personality, such as tolerance, discretion and compassion. I can hardly describe how I appreciate him in a several line.

I am deeply grateful to Professor Susumu Onaka, my co-advisor, for his valuable suggestions on research and his consideration in daily laboratory life. When I had become despondent, he always gave me advices and encouraged me. I would like to express my gratitude to Professor Toshiyuki Fujii for his fruitful advices and suggestions. I have been impressed by his sophisticated advices and ideas for research.

I am deeply indebted to Professors Shinji Kumai, Masanori Kajihara and Yoshisato Kimura for their helpful comments and suggestions.

I would like to express my special thanks to Professor Yoshinao Mishima for his support at the Global-Center of Excellence (G-COE) program. I would like to thank staffs of GCOE program, especially Ms. Hiromi Takahashi and Ms. Mayumi Nakano for their support during the course of G-COE program.

I received generous support from Professors Ryoichi Monzen and Chihiro Watanabe (Kanazawa University) for their assistance in the experiments. Professors Zenji Horita (Kyushu University), Yoshimi Watanabe and Hisashi Sato (Nagoya Institute of Technology) for fabricating UFG Al used in this study.

I would like to thank Dr. Yoji Miyajima who provided valuable suggestions for experiments.

I am thankful to many persons who provided encouragement and assistance. These individuals include

Dr. Yaw-Wang Chai (Tokyo Institute of Technology),

Dr. Yohei Harada (Tokyo Institute of Technology),

Dr. Chiharu Kanno (Mitsubishi Materials Corporation),

Dr. Takahiro Kunimine (Nagoya Institute of Technology),

Dr. Tomotaka Miyazawa (Japan Synchrotron Radiation Research Institute),

Mr. Masato Oshikiri (Mitsubishi Heavy Industries, Ltd.),

Mr. Hiroyuki Tanaka (Mitsubishi Corporation),

Mr. Satoshi Ohizumi (IHI Corporation),

Mr. Hayato Ohta (Nippon Steel & Sumitomo Metal Corporation),

Mr. Hiroshi Kamio (Nippon Steel & Sumitomo Metal Corporation),

Mr. Ryuichiro Shima (Intel Corporation),

Mr. Kazuyuki Tukada (Toyota Motor Corporation),

Mr. Daisuke Shimosaka.

This study was supported by fellowships from the G-COE program (Education and Research Center for Material Innovation) in Tokyo Institute of Technology, MEXT, Japan. I would like to greatly thank to these fellowships.

I would also like to express my appreciation to my mother for her support and encouragements.

February 2013

Yukito NAKANISHI